Int J Mech Mater Des (2014) 10:1–42
DOI 10.1007/s10999-013-9227-9

Shape memory alloy actuator design: CASMART collaborative best practices and case studies

O. Benafan · J. Brown · F. T. Calkins · P. Kumar · A. P. Stebner · T. L. Turner · R. Vaidyanathan · J. Webster · M. L. Young

Received: 10 April 2013 / Accepted: 24 September 2013 / Published online: 24 October 2013

Abstract One goal of the Consortium for the Advancement of Shape Memory Alloy Research and Technology is to compile the collective design experiences of our member organizations into a single medium that researchers and engineers may use to make efficient and effective decisions when developing shape memory alloy (SMA) components and systems. Recent work toward this goal is presented through the framework of six fundamental design aspects we have identified, which include evaluation, alloy selection, processing and fabrication, testing and properties, modeling, and system integration considerations including control system design. Each aspect is documented in the light of enabling the design engineer to access the tools and information needed to successfully design and develop SMA systems. Application of these aspects is illustrated through case studies resulting from our own SMA designs. It is shown that there is not an obvious single, linear route a designer can adopt to navigate the path from concept to product. Each application brings unique challenges that demand a particular emphasis and priority for

O. Benafan (✉)
Structures and Materials Division, NASA Glenn Research Center, Cleveland, OH 44135, USA
e-mail: othmane.benafan@nasa.gov

J. Brown
Dynalloy, Inc., Tustin, CA 92780, USA

F. T. Calkins
The Boeing Company, Seattle, WA 98124, USA

P. Kumar
Department of Aerospace Engineering, Texas A&M University, College Station, TX 77843, USA

A. P. Stebner
Department of Mechanical Engineering, Northwestern University, Evanston, IL 60208, USA

Present Address:
A. P. Stebner
Mechanical Engineering, Colorado School of Mines, Golden, CO 80401, USA

T. L. Turner
Structural Acoustics Branch, NASA Langley Research Center, Hampton, VA 23681, USA

R. Vaidyanathan
Advanced Materials Processing and Analysis Center (AMPAC), Mechanical, Materials, and Aerospace Engineering Department, University of Central Florida, Orlando, FL 32816, USA

J. Webster
Rolls-Royce plc, Derby, UK

M. L. Young
ATI Wah Chang, Albany, OR 97321, USA

M. L. Young
Department of Materials Science and Engineering, The University of North Texas, Denton, TX 76203, USA

each engineering aspect involved in the development of a system actuated by SMAs.

Keywords CASMART · Shape memory alloy (SMA) · Actuator design methodology · Adaptive/active structures · Smart materials, structures and systems

1 Introduction

Shape memory alloys (SMAs) have been a topic of significant research interest for over 40 years (Yamauchi et al. 2011; Otsuka and Ren 2005; Otsuka and Wayman 1998; Buehler and Wang 1968; Cross and Stimler 1969; Jackson et al. 1972; Duerig et al. 1990). Microstructural complexities and their resulting thermomechanical properties have presented challenges in understanding how to integrate these materials into structural applications. Consequently, design of structural and mechanical systems involving SMA materials has been sparse and ad hoc. However, upon examination of a variety of system designs, there are many considerations and parameters that are common to them all. The Consortium for the Advancement of Shape Memory Alloy Research and Technology (CASMART) was established to promote the growth and adoption of SMA actuation technologies by achieving new understanding of the materials, fostering dissemination of technical knowledge, and facilitating application of that knowledge. The Design Working Group of CASMART (CASMART-DWG 2013) strives to serve as a single location to capture the collective best practices, critical information, and perspective necessary for designing material, structural and/or mechanical systems involving SMA actuators. Toward that mission, the objective of this article is to compile the experiences of the authors into a resource that can aid other engineers in SMA actuator development.

The first part of the article is a structured high-level discussion of six aspects critical to SMA actuator system design: 1. *Evaluation* of SMA technology and its applicability to an actuation system (Sect. 2); 2. *Alloy selection* from the wide variety of commercial and research alloys documented to date (Sect. 3); 3. *Actuator fabrication and processing* of the SMA component (Sect. 4); 4. *Testing and properties* that are commonly needed for successful SMA actuation system development (Sect. 5); 5. *Numerical modeling* techniques available to complement empirical development efforts, including first order calculations, engineering models, and constitutive models (Sect. 6); 6. S*ystem considerations*, which encompass system fabrication, SMA component integration, and design of control systems (Sect. 7). The intent of these sections is to capture a broad perspective on development and implementation attributes that affect SMA actuator design and to provide resources for further investigation into each of these topics. In conclusion, six case studies are presented, highlighting the variety in design priorities and processes that arise in developing applications through the common framework of the six design aspects.

2 Evaluation

The main purpose of evaluation is to answer the question: "Does SMA make sense for this application?" Distinct advantages are often found for SMAs in applications where there are space and/or weight constraints, large deformation and/or force requirements, or there is a thermal environment in which energy can be exchanged for benefit, e.g., Duerig et al. 1990; Mavroidis 2002). A combined use of empirical and numerical tools is the most efficient way for designers of all skill levels to assess the viability of SMA actuation for their application. These tools are documented in Sects. 5 and 6.

Evaluating the suitability of SMA can vary from application to application. The following eight questions provide signposts that can direct the evaluation process.

1. *Why use shape memory alloys?* The shape memory behavior of interest must be identified, i.e., the shape memory effect or superelasticity (Ma et al. 2010; Sun et al. 2012; Duerig et al. 1990; Otsuka and Wayman 1998). This behavior should have potential advantages relative to other solutions and technologies.
2. *What are the application requirements?* These requirements will identify what properties and performance characteristics are needed from the SMA element. Applications can require the SMA element to provide a single operational cycle or up

to millions of cycles. Life of an SMA component is driven by the desired response time and thermomechanical loading conditions. These requirements in turn drive the choice of material, form, size, and control methods.

3. *What are the cost/expenditure limits?* The costs include the raw SMA material, processing, and fabrication. The resulting cost per device is critical to the business case for many applications to be commercially viable.
4. *What is the availability and size of the SMA element?* The available input (power) and required output (work) of the SMA element often drive material and form selection. SMA elements can be of a variety of forms (e.g., strips, rods, sheets, wires, springs, tubes, etc.…) in various sizes. Another key consideration is the availability and required volume of the material from a commercial supplier or other source.
5. *What efficiency and response time is needed?* Both energy and mechanical efficiencies of SMA components may be drivers in evaluating SMA technology. However, many applications, particularly in the aerospace industry, are weight sensitive; thus weight savings (mass efficiency) may be of higher priority. The maximum available cyclic frequency can also drive the evaluation.
6. *What is the proposed environment?* The environment, especially thermal conditions, will greatly influence properties of SMAs. Moreover, SMA selection can be limited by the commercial availability of alloys, depending on manufacturing volume of the application. Currently, transformation temperatures are limited to $\sim$115 °C, but this is expected to increase in the near future with the development of high temperature SMAs (Ma et al. 2010; Benafan et al. 2012a). Other concerns may include vibration, humidity, corrosive elements, and bio-compatibility.
7. *What relevant standards and documents are available?* This is especially critical in applications that require certification. Examples of such documents include ASTM standards: F2004-05, F2005-05, F2063-05, F2082-06, F2516-07, F2633-07, application specific documents, certification documentation, and supplier data.
8. *What other components/system will be required?* Finally, the SMA element is often one component in a system that can include other mechanical and electrical elements (see Sect. 8). One must consider if required system integration technologies (see Sect. 7) are available or if development is needed, potentially resulting in increased application cost.

Once SMAs are deemed an advantageous technology for the application, a more detailed design process can begin with some combination of the aspects described in the next sections. Often, a "zeroth-order" model, perhaps consisting of stress and deformation bounds, preferred alloy composition(s), desired geometric form(s), and application constraints may be assembled from answering these evaluation questions and carried into this development.

3 Alloy selection

When developing an SMA actuator, proper material selection is critical to having a successful application. This selection should be based on application constraints and requirements, which include the amount of displacement and force, ambient and actuator temperatures, cyclic stability and fatigue life, and the conditions of the operating environment (e.g., corrosive, oxidizing, etc.).

SMA materials are generally produced by conventional vacuum melting technologies such as vacuum arc re-melting (VAR), vacuum induction melting (VIM), and induction skull melting (ISM) (Russell 2000; Wu 2002). A large variety of compositions and resulting properties exist for known and available SMA materials. Alloy selection is therefore typically driven by the fundamentally different thermomechanical behaviors exhibited by these compositional variations.

The current standard actuator SMA, Nitinol, is a good starting point. Nitinol consists of near-equiatomic compositions of binary nickel-titanium and exhibits an austenite start transformation temperature ranging between −25 °C up to 115 °C, depending on the wt% Ni and thermomechanical processing (Frenzel et al. 2010; Otsuka and Ren 1999, 2005; Otsuka and Wayman 1998; Duerig et al. 1990) (see Sect. 3). Since the binary NiTi alloys are the most common and easily procured actuation alloys, they are often simply identified by the wt% Ni, in the actuator community. Increasing the wt% Ni generally leads to a decrease in transformation temperatures; however, these temperatures can be easily increased by precipitation heat

treatments, which can also have the added benefit of allowing one to tailor other material properties, such as strength and dimensional stability (Sect. 3).The most readily available and well-documented alloys include Nitinol-55 (55 wt% NiTi) composition (Benafan 2012; Stebner 2012; Benafan et al. 2012b, 2013a; Stebner et al. 2013), which was used in the NASA active jet engine chevron (Sect. 8.1) and also the Oxygen Mask Deployment Latches (Sect. 8.3), and Nitinol-60 composition (Hartl et al. 2010c, d; Khamei and Dehghani 2010), as used in the Boeing variable geometry chevron (VGC) (Sect. 8.5).

In addition to binary NiTi alloys, NiTiFe, an alloy which enhances the R-phase by suppressing the martensitic transformation (Duerig et al. 1990; Otsuka and Ren 2005), is readily available on a production level and is commonly used for lower temperature applications, such as the SMA Activated Thermal Switch documented in Sect. 8.4. NiTiNb, is also available on a production level, but is more commonly used for coupling applications (Duerig and Melton 1989). NiTiCu, an alloy which exhibits low thermal hysteresis and improved functional fatigue (Duerig et al. 1990; Otsuka and Ren 2005), has been produced on a production level in the past and was used in the Rolls Royce Gas Turbine Variable Area Nozzle (Sect. 8.6). In the near future, higher transformation temperature materials, such as NiTiPd (Bigelow et al. 2010), NiTiPt (Kovarik et al. 2010), NiTiZr (Gupta 1999), and NiTiHf (Bigelow et al. 2011; Benafan et al. 2012a), are expected to be available (Otsuka and Ren 2005; Ma et al. 2010; Wojcik 2009). These ternary NiTi-based alloys will open doors for higher temperature SMA applications (between 100 and 400 °C), such as aircraft engine components (see Sect. 8.2). While other SMA materials including Co-, Cu-, Fe-, Ni-, and Zr-based alloys (Ma et al. 2010; Wu and Ma 2000) exist, these alloys are less-commonly used as compared to NiTi-based SMAs generally due to limitations either associated with their commercial availability, mechanical properties, transformation temperatures or transformation hysteresis.

4 Actuator fabrication and processing

Once the material has been selected and fundamental properties of the material are deemed appropriate for the application, development of the actuator may commence. This process typically involves selection of an actuator form, processing the actuator to refine thermomechanical performance, and testing to quantify the performance over the parametric space anticipated in the application. In this section, the objective is to highlight key aspects related to fabrication and processing methodologies that transform an SMA from ingot to a useful actuator component.

4.1 Fabrication

Fabrication of SMA actuators requires consideration of 1) actuator form and functionality, 2) fabrication methods, 3) joining techniques, 4) system integration and 5) interrelation between these four aspects, as shown in Table 1. An advantage of SMAs is that the same material can usually be processed into various forms, the most common of which are wire, ribbon, ring, bar, rod, foil, sheet, spring, tube, and plate. Conventional metalworking processes such as forging, rolling, and extrusion are used to achieve fabrication of SMA mill products. Depending on the form, SMA actuators can generate motion in one dimension, such as in the case of a thin-wire form (Dolce and Cardone 2001) (see Sects. 8.1 and 8.3), in two dimensions, such as in bending of a bar (Wessels et al. 2012) (see Sects. 8.5 and 8.6) or even motion in a more complex three-dimensional manner, such as in largely deformed springs (see Sects. 8.2 and 8.4), honeycomb (Grummon et al. 2006), or micro-bump structures (Sun et al. 2009). Form selection is dependent on element functionality or actuation method. Tension (e.g., wires, springs), compression (e.g., rods, springs), bending (e.g., beams, plates) and torsion (e.g., rods, tubes, and springs) loading modes have all been exploited in some form based upon the desired functionality.

Fabrication processes that will not satisfy the actuator development requirements may be ruled out using screening methods through a fabrication-processes-first approach (Dixon and Poli 1995; Eggert 2005). This approach helps in eliminating the fabrication processes that will not satisfy the actuator development requirement. Such requirements could be geometric complexities, actuator size or production volume. Table 1 identifies three major fabrication method categories. Material removal processes including mechanical machining (milling, drilling and turning), laser or water-jet cutting, etching/electropolishing and electrical discharge machining

Table 1 SMA actuator fabrication processes with examples

Fabrication

Actuator form & functionality				**Fabrication methods**	
	Example		*Example*	*Material removal*	*Example*
Wire	Novak et al. (2008) and Young et al. (2010)	Plate	Mohammad et al. (2002)	Mechanical machining (milling, drilling, turning)	Weinert and Petzoldt (2004) and Weinert et al. (2004)
Bar	Olsen et al. (2012)	Beam	Hartl et al. (2010c)	Laser beam/water jet	Kong et al. (2011)
Sheet	Kohl et al. (1999)	Tendon/ Cable	Reedlunn et al. (2009, 2010), Reedlunn and Shaw (2008) and Redmond et al. (2008b)	Etching/ electropolishing	Man and Zhao (2006)
Ribbon	Mehrabi et al. (2012)	Truss	Savi et al. (2002) and Bandeira et al. (2006)	Electrical discharge machining (EDM)	Theisen and Schuermann (2004) and Hsieh et al. (2009)
Spring	Stebner et al. (2008), Benafan and Vaidyanathan (2009), Mirzaeifar et al. (2011) Grossmann et al. (2008) and Frenzel et al. (2011)	Honeycomb	Grummon et al. (2006) and Hassan et al. (2008)	*Deformation processes*	
Tube	He and Sun (2009) and Favier et al. (2007)	Foam	Li et al. (2009), Bertolino et al. (2011), Bansiddhi and Dunand (2007), Ipek Nakas et al. (2011), Resnina et al. (2013), Neurohr and Dunand (2011), Aydoğmuş et al. (2011) and Young et al. (2012)	Hot forming (forging, rolling, extrusion)	Maziarz (2008) and Foroozmehr et al. (2012)
				Cold forming (wire drawing, swaging)	Zhang et al. (2013), Atli et al. (2011) and Wu et al. (2000)
Joining Techniques				*Consolidation processes*	
	Example			Powder metallurgy/ sputtering	Pourkhorshidi et al. (2012)
Welding	Friction welding (Fukumoto et al. (2010)			Bonding	
Laser welding (Li et al. 2013; Chan and Man 2011)					

Table 1 continued

Fabrication			
Soldering/brazing	Grummon et al.(2006) and Li et al. (2007)	**System integration**	
Mechanical joining		Attachment location	
Crimping		Finishing	See Case studies
Adhesive	Antico et al. (2012) and Smith et al. (2004)	Assembly	

(EDM) are processes that generally involve wasted material that increases the total fabrication cost. Deformation processes including hot forming (e.g., forging, rolling, extrusion) and cold forming (e.g., wire drawing, swaging) are processes that change the shape of the raw material by rearranging the solid. Consolidation processes such as powder metallurgy, sputtering, plasma spray and bonding are processes that combine powder or small sub-parts together.

Actuators with complex shape and properties often involve more than one fabrication process. Sometimes, complete fabrication requires joined assemblies of two or more components. Various joining techniques are available but only a few have been shown to be effective (e.g., Falvo et al. 2005; Li et al. 2012, 2013; Yan et al. 2006). Welding SMA to SMA can be effective, but also problematic. Common concerns associated with welding are embrittlement, thermal-induced residual stresses and changes in properties. Nitinol can be welded to itself using traditional spot welding techniques. Acceptable joint strengths can be achieved when the welding is done in an inert-gas environment, e.g., argon, to avoid formation of brittle oxides (see Case study—8.1). Soldering and brazing are other commonly adopted joining techniques. Brazing has been demonstrated as an effective method to join Nitinol to itself through the use of a Ag-rich barrier layer to prevent the formation of brittle intermetallics like $NiTi_2$ (see Case study—8.6) (Shiue and Wu 2006). Soldering/brazing fluxes reduce concerns about the heat affected zone and provide closer assembly tolerances and a neater joint appearance. However, the composition, strength and melting point of the assembly can be altered. When permanent joints are to be avoided, mechanical fastening is an option. Several mechanical fasteners are available including integral fasteners (e.g., flanges, embossed protrusions and crimps), discrete fasteners (e.g., screws, inserts, studs, and rivets), seams, press fits, shrink/expansion fits and more. Although mechanical fastening provides easy disassemble and reassemble without affecting the base material properties, concerns such as misalignment, stress concentrations and environmental conditions can be an issue.

4.2 Processing

In conjunction with the fabrication and joining processes presented above, actuator structure and

properties can be further tuned through processing. Actuator processing serves to change component structure or properties, or to restore those that were altered during fabrication. In nearly all actuator applications, heat treatments and thermomechanical training are employed.

A variety of heat treatments may be used to alter actuator structure and properties. Shape setting is a thermo-mechanical process employed in creating most SMA actuators. A common practice for shape setting (Hodgson 2000; Smith and Hodgson 2004; Benafan et al. 2013b) entails (1) mechanically constraining the fabricated material (wire, sheet, tube, etc.) within a fixture of the desired shape, (2) heat treating the constrained material at a high temperature for a dwell time (commonly at 500 °C for 1 h. for NiTi), (3) cooling the material (vacuum, air, or quenching) and finally (4) optimizing the final geometry through subsequent shape sets or additional machining.

In addition to shape setting, other heat treatments are often used to elicit precipitate structures that tune properties such as yield strength, dimensional stability, and transformation temperatures, or to relieve internal stresses (Otsuka and Ren 1999, 2005; Otsuka and Wayman 1998; Somsen et al. 1999; Kim and Miyazaki 2005; Nishida et al. 1986). For instance, NiTiHf alloys produced by NASA GRC were prepared by VIM (Bigelow et al. 2011; Coughlin et al. 2012; Benafan et al. 2012a). The ingots were vacuum homogenized for 72 h at 1,050 °C and furnace cooled followed by hot extrusion at 900 °C and an area reduction ratio of 7:1. Samples (in final form) were then subjected to an aging treatment at 550 °C for 3 h and furnace cooled. This heat treatment was selected after a previous optimization study of different aging temperatures and times, where it was found that these conditions provided the best thermomechanical properties (Bigelow et al. 2011; Coughlin et al. 2012).

As mentioned at the beginning of this section, thermomechanical training processes are used in addition to heat treatments to establish stabilized actuator performance for application-specific operational and environmental conditions. These training processes often entail a series of load-bias cycles (thermal cycling through the phase transformation temperatures under constant stress), strain-bias cycles (thermal cycling through the phase transformation temperatures under constant stress), or specialized training routines such as one time loading, minor loops and others. These methods are designed to impart cycle-to-cycle mechanical stability, a property that dramatically influences functional fatigue of the actuator. This is critical to fail-safe design, safe operation, reliable performance and the life of the SMA actuator in the application.

5 Testing and properties

Determination of the optimal operating stress boundaries and other critical material properties is required for successful design. To date, testing methodologies, data interpretation, and terminologies used to describe tests and material properties have varied greatly, which often lead to uncertainty or misinterpretation when comparing material properties and data acquired from different sources. Processes have been established and incorporated into ASTM standards (F1387-99, F2004-05, F2005-05, F2063-05, F2082-06, F2514-08, F2516-07, F2633-07, F2754-09) for many isothermal (body temperature) or bithermal (room temperature & body temperature) superelastic applications to address this issue, but at this time there are no standards for thermomechanical actuation applications. Thus, in this section we propose unified procedures for testing and determination of SMA thermomechanical properties, along with general definitions and terminologies. The properties of interest for actuator design may be broadly categorized as (i) effective thermoelastic properties, (ii) transformation stresses and temperatures, (iii) durability and (iv) other properties and additional factors.

5.1 Effective thermoelastic properties

Thermoelastic properties that are prevalent in SMA actuator design are most often obtained from isothermal monotonic mechanical deformation tests as well as thermally cycling through the phase transformation under a constant applied load (e.g., Bigelow et al. 2010, 2011; Duerig et al. 1990; Otsuka and Wayman 1998). Geometries used to obtain these properties span the gambit of mechanical test specimens including wires, cylinders, parallelepipeds, cylindrical and rectangular "dogbones", and tubes. The chosen specimen geometry and orientation with respect to processing and the loading mode (e.g., tension, compression,

torsion, combined) should mimic the application as closely as possible. This recommendation arises from large inelastic contributions to SMA deformations and asymmetric responses with respect to loading mode. Additionally, materials used to create actuators, especially cold worked geometries such as wires and tubes, are generally anisotropic due to significant texture (e.g., Bhattacharya 2003; Bhattacharya and Kohn 1997). Thus, generally Hooke's law may not be adopted to transpose axial material properties to shear properties and is not possible to infer tensile properties from a torsion test or vise versa.

Loads are measured using force transducers and, when it is appropriate, they are normalized by the initial cross-sectional area of the gauge section to facilitate data reporting in units of stress. Traditional contact extensometers, contactless laser devices, or digital cameras with digital image correlation software are recommended for measuring strains (Favier et al. 2007). The contactless methods are often preferred as they are more adaptable to observing the large deformations that are characteristic of SMAs. Strain gauges (i.e., Wheatstone bridges) are not recommended for measuring average strains of SMA specimens since the phase transformation in these materials often nucleates and propagates in a heterogeneous manner (Shaw 2000; Shaw and Kyriakides 1997b; Olson and Cohen 1972; Olson and Owen 1992). Furthermore, moving fronts during transformation, localization of multiple nucleation sites, or improper contacts often result in data that does not represent the average behavior of the specimen when using strain gages. Such heterogeneous and transient behavior in mechanical testing of SMAs has been observed via optical techniques like infrared thermography (Favier et al. 2007; Gollerthan et al. 2009; Shaw and Kyriakides 1997a, b; Iadicola and Shaw 2002) and digital image correlation (Favier et al. 2007; Iadicola and Shaw 2002).

Different choices of load path parameters used in testing, such as load/stroke rates and control modes (i.e., stress, strain, load, or displacement control), will lead to very different SMA responses. This is because the inelastic deformations that dominate SMA actuation exhibit strong rate sensitivity. Thus, the loading rate and control mode used in the test should mimic those desired in the application as closely as possible. For example, if a strain control mechanical test is being used to determine properties, the equation ($\dot{\varepsilon} = \frac{\varepsilon}{t}$) can be used to identify a strain rate $\dot{\varepsilon}$ where t is the time over which each actuation cycle will occur in the application and ε is the desired actuation strain. Analogously, $\dot{T} = \frac{\Delta T}{t}$ can be used for temperature control where $\dot{T}$ is the temperature rate and ΔT is the desired change in temperature for the required actuation strain. For load control cases, the equation ($\dot{F} = \frac{\Delta F}{t}$) can be used where $\dot{F}$ is the force rate and ΔF is the desired change in force for the required actuation strain. Many SMA actuators, however, experience a mixed–mode control situation in service due to a variety of boundary conditions that are a consequence of non-SMA components of the actuator design, such as incorporation of hard stops to control the actuator stroke or use of a spring to "bias" the unactuated position (Dynalloy 2011) (see Sect. 8 for examples). Therefore, actuator design is most accurate when the tests to acquire material properties as well as the test equipment most closely mimic the intended use in the application. If the control mode of the application is unknown at the time of testing, it is recommended to use displacement or strain control over load or stress control since the inelastic deformation plateaus, which are characteristic of SMA responses (see Fig. 1), take place over a very small load/stress increment but a moderate displacement/strain increment. Thus, displacement/strain control will provide better resolution over the whole of the deformation responses.

Temperature control must also be considered when testing SMAs both in the isothermal and cyclic test conditions. Induction units, furnaces, cartridge heaters, thermal pads and Joule heating (electrical current)

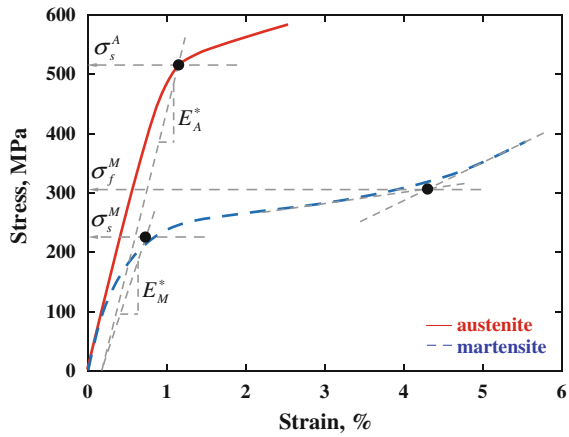

Fig. 1 Example of effective elastic property evaluation. (Color figure online)

are some of the common methods used to heat SMA specimens. Cooling to sub-ambient temperatures is typically accomplished via an environmental chamber and liquid nitrogen. In all cases, a uniform temperature distribution must be maintained across the gauge section with variations limited to within 1 % of the test temperature.

Thermography or some other non-contacting temperature measurement method is preferred for sensing specimen temperature. Surface emissivity of the SMA specimen is typically required for non-contacting temperature measurements. Emissivity can be measured by standard techniques, e.g., ASTM E1933, and typically varies with surface condition. Thermocouple temperature measurement is possible if non-contacting measurement is not practical. The finest gauge thermocouple wire possible should be used to minimize the influence of the thermocouple on the measurement. The spot-weld should be performed in an inert environment, e.g., argon, to avoid production of brittle oxides. Other methods of thermocouple attachment include soldering and bonding. Soldering requires a local area of cladding (e.g., Cu) on the SMA and bonding should be accomplished via a thermally conductive adhesive. All of the contacting temperature measurement techniques affect the performance of the specimen and are prone to temperature measurement error.

It is recommended to conduct at least one test to verify the gradients across the gauge length of the specimen (e.g., using multiple thermocouples or thermal cameras). When testing bulk samples, especially when using induction heating, samples must be heated throughout the volume of the specimen, not just the surface where the thermocouple is attached. This is normally achieved by properly designed induction coils (geometry, coil spacing, frequency), or by allowing a soak time at a temperature. Heating/cooling rates have been shown to have an effect on the thermomechanical response of these alloys. Heating rates of 20–30 °C/min are typical values used, and can be controlled using a tunable temperature controller. Besides free convection, cooling is usually achieved by forced convection (e.g., vortex tubes, air lines), cooling jackets with chilled fluid (e.g., water or liquid nitrogen), or with controlled fluid baths.

While inelastic mechanisms contributing to SMA properties differ (Qiu et al. 2011; Qiu and Krishnan 2009; Benafan 2012; Stebner et al. 2013), their effective properties are analogous to those of other structural materials. Thus, graphical methods similar to those used for other metallic materials may be incorporated. The effective Young's modulus (E^*) of the austenite and martensite phases can be determined from fitting the initial loading responses of each phase, as shown in Fig. 1. It is also common practice to measure these properties from the unloading portion of the curves, but both approaches tend to yield similar results when only effective values are sought. When measuring the austenite modulus (E_A^*), the ideal method is to conduct the test at temperatures above the M_d temperature (temperature where no stress-induced martensite can form). Some materials, however, such as Nitinol-55 exhibit the same initial linear elastic response as long as the test temperature is above $A_f + 25$ °C, i.e., tests above the M_d temperature are not required (Benafan 2012).

The effective thermal expansion coefficients of the material, α_A^* and α_M^*, can be measured from observing the pure austenite and pure martensite strain temperature slopes of a zero-load thermal cycle as shown in Fig. 2 (Qiu and Krishnan 2009). Traditionally, effective Poisson's ratios, v_A^* and v_M^*, have been assumed (Otsuka and Wayman 1998; Lagoudas 2008), though measurements of Poisson's ratios have recently been reported for NiTi (Qiu et al. 2011; Stebner et al. 2011; Young et al. 2010).

5.2 Transformation stresses and temperatures

Unlike conventional materials, SMAs require cyclic thermal tests in additional to isothermal, monotonic and cyclic mechanical experiments in order to define the actuation-specific properties. Cyclic thermal tests are typically called "load-bias" tests and refer to a test in which a specimen is thermally cycled through phase transformation under constant applied load/stress. A characteristic strain-temperature response resulting from load-bias cycling of an SMA is shown in Fig. 3. The actuation-specific properties include transformation strain, work output, residual strain, transformation temperatures and hysteresis. There are four characteristic temperatures associated with the phase transformation. On the initial heating portion, martensite starts to transform to austenite at the austenite start temperature (A_s) and completes transformation at the austenite finish temperature (A_f). Similarly, during cooling, the forward transformation initiates at the martensitic start temperature (M_s) and finishes at the

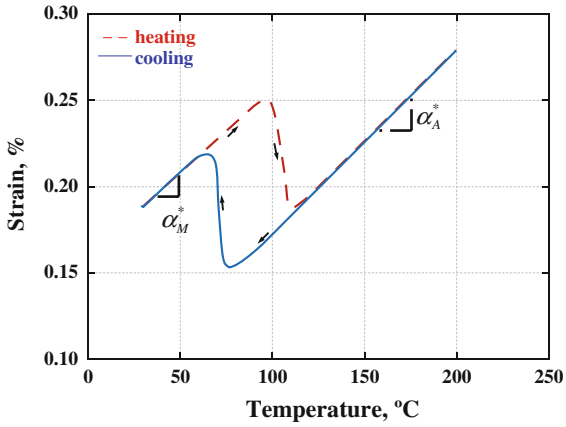

Fig. 2 Example of effective thermal expansion coefficients evaluation. (Color figure online)

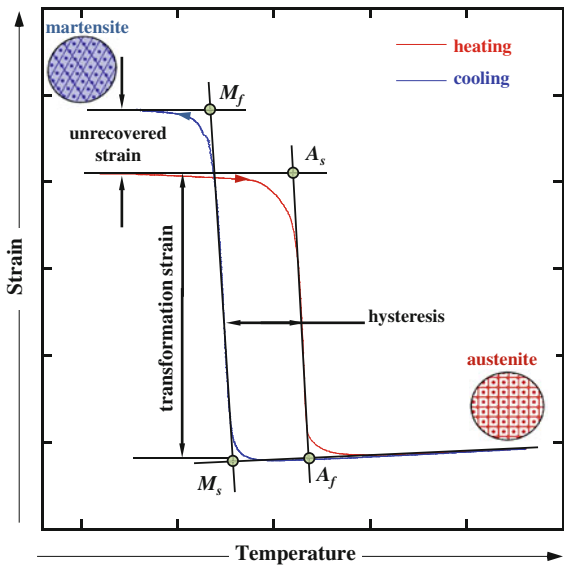

Fig. 3 Characteristic load-bias test showing transformation-specific properties. (Color figure online)

martensitic finish temperature (M_f). These temperatures are typically measured using the tangent-intercept method as described in the ASTM standard (ASTM-F2082-06 2010). The transformation strain, a measure of the work output of the material, is calculated as the difference in axial strain measured by the intersection points for the heating portion of the thermal cycle. Transformation strain is also used to calculate work output as the product of applied engineering stress and transformation strain. The residual strain, a measure of the dimensional stability, is determined by measuring the strain difference between the beginning and end of the thermal cycle, either at the low or high temperature side. In an ideal case, this residual strain would be zero and the actuator would return to the same position in each cycle. Finally, the hysteresis can also be measured by taking the temperature difference between the forward and reverse transformation.

Knowledge of transformation temperatures and critical stresses, as well as temperature-stress relationships is essential for actuator development. The analog of yield stress determination for non-SMA materials may be incorporated to determine some critical stresses. That is, a 0.2 % strain-offset method can be used to determine the onset stress for reorientation of the martensite phase (σ_s^M) and the onset stress for stress-induced transformation of the austenite phase (σ_s^A), as shown in Fig. 1. To determine other inflection points, it is often common practice to adopt the "tangent intersection method" (ASTM-F2082-06 2010). For example, in Fig. 1 this method is used to observe the stress at which martensite reorientation begins to saturate (σ_f^M). These initial and saturation stresses are indicted by σ_s and σ_f on the phase diagram in Fig. 4. Generally speaking, they are critical to design for actuation applications because very little transformation strain will be exhibited by the SMA component at stresses below σ_s and maximum transformation strain will be achieved at stresses above σ_f. There are exceptions and limitations to these generalities. For instance, transformation strain can be

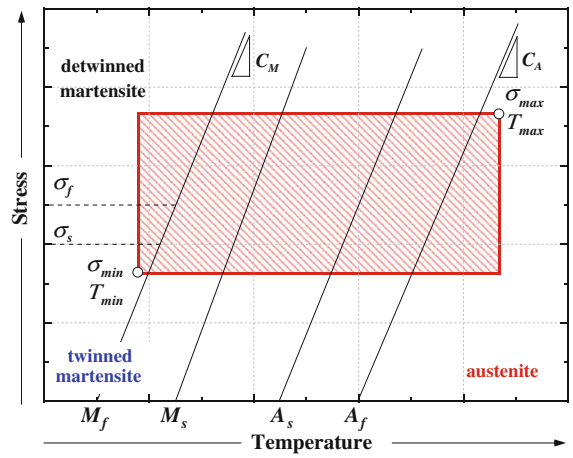

Fig. 4 Stress-temperature phase diagram—*red box* bounds a typical actuator design space. Consideration of transformation temperatures relative to environmental temperatures is crucial to successful alloy selection. (Color figure online)

achieved at low stresses, below σ_s, through the two-way shape memory effect. Also, SMA performance will start to deteriorate if the material is subjected to stresses significantly higher than σ_f.

In Fig. 4, the four surfaces that represent the phase transformation regions separate the pure-austenite phase from the martensite phase. These transformation surfaces can be linear, quadratic or of a higher-order, non-linear form depending on the material system, processing and thermomechanical treatment. For simplicity, they are often approximated as linear, as in Fig. 4, and each surface is characterized by the slope relating the shift of a transformation temperature with different levels of applied stress. These slopes are described by "Clausius-Clapeyron" coefficients (e.g., C_A, C_M). Stress-free transformation temperatures are traditionally determined by conducting a simple differential scanning calorimetry (DSC) analysis (ASTM-F2004-05 2010). However, for developing an actuator application, it may be desirable to instead determine them through a load-bias test at very low stress ($\sigma_{eng} < 5$ MPa). In choosing the latter method, the same specimen may then be used for a series of load-bias tests, as shown in Fig. 5. From this series, the tangent intersection method may be used to determine transformation temperatures and their relationship to applied stress (hence C_A, C_M as shown in Fig. 4).

5.3 Durability

Durability testing is critical towards understanding the structural and/or functional fatigue life of SMAs.

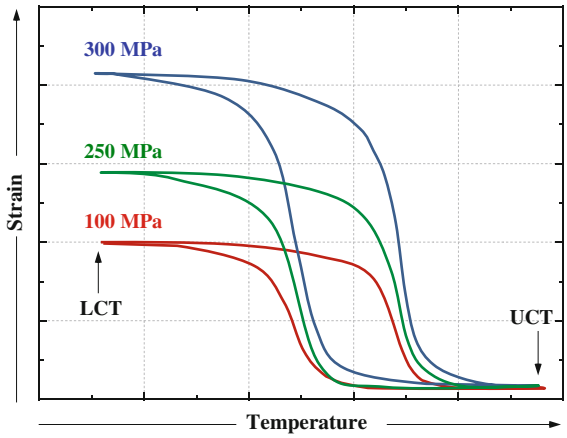

Fig. 5 Load-bias tests at different stress levels. UCT and LCT are the upper and lower cycle temperatures, respectively. (Color figure online)

Structural fatigue of the SMA refers to the mechanical failure or fracture of the SMA component, which typically originates at inclusions, stress concentrations, surface imperfections, or thermal "hot spots" within the component. Functional fatigue refers to operational failure of the SMA component within the application, which is often not associated with structural fatigue (Eggeler et al. 2004; Wagner et al. 2004; Casati et al. 2011). The most common functional fatigue modes are drift in the transformation temperatures, accumulation of residual strain and decay of actuation strain over a number of cycles (Gall et al. 2008; Tobushi et al. 1997; Gloanec et al. 2010; Figueiredo et al. 2009).

There are several parameters that must be studied to acquire a detailed understanding of durability. The surface-finish-to-specimen-thickness ratio is critical for structural failure but not functional fatigue (Patel and Gordon 2006). The surface finish must be addressed relative to the specimen geometry in fabrication (see Sect. 4, Table 1) and sufficient to avoid initiation of fracture from surface features such as oxides. Functional fatigue life may be assessed by performing cyclic tests that closely mimic the intended loading and biasing of the SMA component. During testing it is preferred that the upper cycle temperature (UCT) and lower cycle temperature (LCT), illustrated in Fig. 5, be chosen from the bounds for the load-bias tests to closely mimic the temperature bounds desired in application, as the UCT and LCT dramatically affect the actuation response of many SMAs, including binary NiTi (Padula II et al. 2012).

In summary, documentation of the following parameters is a minimum recommendation in reporting fatigue data:

- Specimen geometry and dimensions;
- Upper and lower cycle temperatures;
- Power source and control signal;
- Heating and cooling rates (independently, not simply total frequency);
- Load modes, levels, and rates;
- Ambient temperature and special thermal boundary conditions, such as use of a bath;
- Bias type and force;
- Any use of hard stops.

In the event of thermal gradients experienced within the specimen gauge length, it is important to additionally report the temperature gradient in the

specimen in all 3 directions, and the maximum/minimum temperature experienced by the specimen.

5.4 Additional properties and other factors

Additional tests to determine performance of the SMA component under shock loads or in a corrosive environment may be required (Zurbitu et al. 2010; Bertacchini et al. 2003), depending on the requirements of the application. In all SMA testing and data interpretation, it is important to understand the processing history (see Sect. 4) of the component and consider the effects it may have on the observed responses. Heat treatments, machining processes, specimen geometry, and cold work all have the ability to alter SMA behaviors. Thus, care must be taken in interpreting data for application design (Schaffer and Plumley 2009; Lagoudas et al. 2009).

6 Numerical modeling

While fundamental tests and material property determination can aid application design, it is often desirable to use some combination of modeling and empirical observation of the desired SMA component performance for design validation as use of numerical tools may reduce the development times and costs of SMA components. In a product development cycle, there are several occasions where it may be advantageous to perform a calculation or simulation. The earliest is in the evaluation stage (see Sect. 2). Here analytic formulae and numerical models provide a means for evaluating whether or not an SMA is able to deliver a desired performance. However, numerical tools are perhaps even greater assets in selecting the final configuration and geometric parameters of the SMA component (e.g., Gravatt et al. 2010; Hartl et al. 2010a, c; Stebner et al. 2008, 2009; Turner 2005), developing SMA control parameters and algorithms (e.g., DeCastro et al. 2007; Cui et al. 2010; Chen et al. 2009; Song and Ma 2003, 2007; Song and Quinn 2004; Ma et al. 2004; Ma and Song 2002, 2003; Song 2001b, 2002; Song et al. 1999, 2000, 2001, 2003a, b, 2011; Furst and Seelecke 2012), and understanding the interaction of the SMA component with the rest of the actuation system and its environment (e.g., Burton et al. 2006; Davis et al. 2008; Oehler et al. 2012b; Turner 2001).

Readily available tools for calculating SMA actuation include manufacturer supplied material properties (e.g., Dynalloy 2011), engineering models (e.g., Duerig et al. 1990; Redmond et al. 2008a; Otsuka and Wayman 1998), and SMA constitutive models (e.g., Turner 2000a, b; Lagoudas 2008; Hartl and Lagoudas 2009; Panico and Brinson 2007; Seelecke 2002; Chemisky et al. 2009; Saleeb et al. 2011; Gao and Brinson 2002; Lagoudas et al. 2006; Patoor et al. 2006; Kelly and Bhattacharya 2012; Stebner and Brinson 2013; Turner and Patel 2005, 2007). These tools vary in complexity, capability, and accuracy. Knowing how to select the most efficient tool for a desired outcome requires some knowledge of both SMAs and the tools themselves. Thus, there are current efforts focused on documenting the tool selection process (Hartl et al. 2012). When coupled with the previously described experiments, parametric design tools provide an ability to optimize actuator parameters at a fidelity that is often not practical to achieve solely through empirical studies. In the remainder of this section, we briefly review numerical tools that are available for parametric studies.

6.1 First-order calculations

If commercially supplied or some other well-documented material is being used, first-order parametric evaluation may be performed through calculations using vendor-supplied or previously determined properties and relationships between properties and geometric parameters. In some instances, such as in NiTi wire design, this may be sufficient for the entire project. For example, if buying actuator wire from Dynalloy, their “Tech Sheets” document (Dynalloy 2011) provides both electrical and mechanical properties for their entire family of alloys used in six common wire actuator configurations. These sheets provide all of the information necessary to select the proper wire diameter, length, and biasing component for the SMA actuation mechanism, as demonstrated in the Oxygen Mask Deployment Latch case study (Sect. 8.3). However, if developing an application using a configuration or alloy that is not widely available on the commercial market, it is not likely that there will be vendor-supplied data and guidelines available. For parametric refinement in these cases one must adopt some type of model that may be fit by empirical data to

interpolate and/or extrapolate beyond the experiments that have been carried out in the development cycle.

6.2 Engineering models

Where first-order calculations are unavailable or insufficient, engineering models are often developed from empirical data to facilitate selection of final design parameters. Such models were used in designing the SMA Activated Thermal Switch (Sect. 8.4) and Gas Turbine Variable Area Nozzle (Sect. 8.6). One common way to develop an engineering model is to first create SMA test specimens in the likeness of a non-SMA mechanical component that is thought to be of use for the application, such as a spooled wire (Redmond et al. 2008a) or a helical spring (Otsuka and Wayman 1998; Duerig et al. 1990). Then the responses of the austenite and martensite phases of the SMA in this configuration are observed through testing. To create the numerical model, parameters are fit and/or new parameters are introduced to the engineering or graphical model for the analogous non-shape memory component such that the empirical response of each phase is replicated, and the difference between the two provides the transformation properties.

Development of these models is well established in SMA actuator design, having been documented in published texts on the subject (Otsuka and Wayman 1998; Duerig et al. 1990). One limitation of these tools is that they are constructed using formulae of linear elastic theory, yet they are describing highly inelastic phase transformations and martensite deformations. They work well to interpolate between data for SMA actuations comprised of deformations that fit within the confines of small-strain theory to first-order approximation (see (Malvern 1969) or another mechanics text for more on small-strain theory). However, they have a propensity to be inaccurate if used to extrapolate outside of the data that is used to calibrate them or to describe large shape changes or highly nonlinear material responses (Stebner et al. 2009). Still, provided that data is available to calibrate the models at the boundaries of intended use, they are a very quick, simple, and efficient means to refine the parameters of simple geometries subjected to a single mode of loading, as in the case of torque tubes in torsion-only or wires in tension.

6.3 Constitutive models

SMA constitutive models implemented into numerical codes provide a robust means to extrapolate and interpolate across large parameter spaces with little required experimental input. Constitutive models were adopted or developed in designing the active jet engine chevron (Sect. 8.1), the VGC (Sect. 8.5) and the Gas Turbine Variable Area Nozzle (Sect. 8.6). Many different constitutive models have been developed to simulate SMA behaviors over the course of the past 30 years. These range from microstructure models that can be used to study and predict effects of composition and processing (e.g., Gao 2002; Gao and Brinson 2002, 2000; Gao et al. 2000, 2005; Stebner et al. 2011; Huang and Brinson 1998; Huang et al. 2000; Patoor et al. 1993, 1994; Sun and Hwang 1993; Thamburaja 2005; Thamburaja and Anand 2001) to phenomenological continuum models with a wide variety of features developed specifically for engineering components and devices (e.g., Turner 2000a, b; Lagoudas 2008; Hartl 2009; Panico and Brinson 2007; Seelecke 2002; Saleeb et al. 2011; Achenbach and Muller 1985; Arghavani et al. 2010; Boyd and Lagoudas 1996, 1999; Brinson 1993; Brocca et al. 2002; Hartl et al. 2010b; Kelly and Bhattacharya 2012; Lagoudas et al. 2006; Patoor et al. 2006; Stebner and Brinson 2013; Tanaka and Iwasaki 1985; Turner and Patel 2005, 2007).

Models of the latter class may be implemented such that they interact with commercial finite element software; hence they are often the most logical choice for modeling of SMA actuator components, especially those of complex configuration or those subjected to multi-axial loading or nonlinear deformations. These models are not without limitations, so one should be sure to understand the theories, assumptions and intended use of the constitutive model before selecting it for their actuator design process. For example, many constitutive models have been developed, validated, and verified only for superelastic behaviors (e.g., Lexcellent and Bourbon 1996; Morin et al. 2011a, b; Sadjadpour and Bhattacharya 2007). Thus they may not have the ability to properly simulate actuation. However, several research groups have put great efforts into developing and vetting models for actuation (Turner 2000b; Lagoudas 2008; Hartl 2009; Panico and Brinson 2007; Saleeb et al. 2011; Arghavani et al. 2010; Bo and Lagoudas 1999; Boyd and

Lagoudas 1996; Brinson 1993; Brocca et al. 2002; Hartl et al. 2010b; Kelly and Bhattacharya 2012; Lagoudas et al. 2006; Patoor et al. 2006; Stebner and Brinson 2013).

In selecting an SMA constitutive model, the designer should first understand SMA characteristics that are critical to the component they are designing. The simplest model capable of replicating these characteristics should be selected. For instance, if designing a rod actuator only subjected to tension, a one-dimensional model (such as Brinson 1993) can be chosen as opposed to a three-dimensional model. Similarly, if designing a porous structure, a three-dimensional model formulated to handle phenomena such as multi-axial loading and load redistribution about pores would be required (e.g., Panico and Brinson 2008). If using a highly cold-worked SMA structure such as a drawn tube, the ability to simulate material anisotropy (i.e., different material properties along the tube axis versus the radial direction as in Kelly and Bhattacharya (2012) may be required for accurate results. Through a few simulations, a designer may quickly evaluate performance characteristics such as maximum stresses, transformation strains, and also gain a sense as to the benefits and consequences of changing geometric parameters. As with finite element analyses of non-SMA components, a greater design space may be explored at a higher resolution by linking the finite element simulations with design and optimization software packages (Hartl et al. 2011; Oehler et al. 2012a).

7 System considerations

Final design of an SMA actuator requires consideration of system integration factors. Such factors may include the manner in which the actuator is joined with the rest of the system, thermal management, and control methodology.

7.1 Fabrication and integration

Integration of SMA actuators into structural and/or mechanical systems can involve many factors. Perhaps foremost in importance is consideration of whether the SMA actuator is distinct from (attached only discretely, e.g., Case study—8.4) (Benafan and Vaidyanathan 2009) or integrated with (attached, bonded or embedded in a continuous manner, e.g., case study—8.1) other parts of the system. This SMA actuator integration attribute affects many other system integration factors.

Attachment provisions are a primary concern in either the distinct or integrated actuator case. Options include mechanical connections (i.e. crimping wires, see Sect. 8.3, Dynalloy 2011), bonding, welding and brazing. Mechanical connections are the simplest type and are most common in applications involving distinct SMA actuators or where electrical connection is desired. Mechanical connections and techniques for joining SMA to SMA were discussed in the Sect. 4. Similar techniques involving mechanical connections, welds or brazed joints are often used when integrating the actuator into a mechanical or structural system. An exception is when the actuator must be bonded to or embedded within a fiber-reinforced polymeric (FRP) structure.

Techniques used for bonding an actuator to the exterior of a structure and embedding one within a polymer-based composite structure are similar. Structural adhesives include epoxies, acrylics, silicones and hot melts. Bonds with adhesives and composite resins can often be rendered effective through simple mechanical means such as light sandblasting or chemical etching to remove the oxide layer. Even greater bond strengths can be achieved through a more sophisticated process of etching and priming the SMA actuator to achieve a combined mechanical and chemical bond. One such method involves cleaning with an organic solvent, grit blasting, acid treatment for new oxide formation and chemical bonding with a Silane coupling agent, such as amino siloxane (Dow Corning Corporation 2009; Sever et al. 2009; Smith et al. 2004). As with many joining method, adhesive bonding disadvantages consist of poor impact properties, instability at relatively low temperatures and chemical reactions.

In many cases, SMA actuators work against a deformable structure or articulating mechanism. Although two-way shape memory can be implemented to enable reversible control of an actuated system, greater stroke and force can be achieved by employing two one-way shape memory elements as an agonist–antagonist pair and/or by using a non-SMA bias element in the system. Implementation of agonist–antagonist pairs can be complicated by the need for thermal isolation between actuators. The bias-element approach is more common and can be achieved via a

conventional spring or a deforming structure, both of which provide a restoring force to return the SMA actuator to the rest configuration.

Heating by direct current requires access to the actuator ends and is dependent upon electrical resistance (see Alloy selection and Case study—8.1) that is compatible with the power source. Actuator access locations and electrical resistance can both be controlled as desired by forming electrical circuits via joints (e.g., mechanical connectors, welds, brazing) between multiple SMA actuators. Other means of active applied heating include surface-mounted and cartridge heaters that can be bonded or inserted into SMA actuators, or by induction/eddy current heating (Butera and Bianconi 2000).

For direct-current heating, power transmission wires should be routed as directly as possible to minimize resistive load and wire gauge should be adequate to carry the required current to the SMA actuators without introducing parasitic losses. Connectivity to the SMA actuators can be achieved through mechanical connections or a better and more permanent electrical connection can be achieved through soldering. An acceptable solder joint requires cladding (e.g., Cu) of the SMA actuator. Cu cladding can be accomplished by standard industrial electroplating processes. Although the impedance of SMA actuators can be controlled by development of clever circuitry, as mentioned above, the load is primarily resistive and requires a power source that can deliver adequate current for heating.

The rate at which heat can be dissipated from the SMA actuators to the environment is the dominant factor in determining frequency response of the system. Environmental heat loss can be improved by optimizing conductive, convective and, to a lesser extent, radiative heat loss paths. This must be balanced, however, with requirements for heating the actuators. Devices that are useful for improving heat loss include finned heat sinks, heat pipes and thermoelectric modules. Improvements in frequency response can be achieved by a thermal control approach involving active cooling as well as heating. Active cooling is possible through thermoelectric modules and directed forced convection.

Mechanisms have an important role in many applications. Levers and linkages are most prevalent due to the ability to amplify stroke or force. Locks, brakes and over-center devices are other mechanisms that have proven useful in conjunction with SMA actuators for some applications.

7.2 Controls

A critical element of an SMA actuation system is control methodology (Gedouin et al. 2011; Williams et al. 2010). Control of SMA actuators is typically implemented by active or passive means of applying and removing heat. Perhaps the most elegant applications of SMA actuators are those that use changes in ambient conditions to control the SMA actuation, or passive control. More typically, however, active control is achieved through applied heat and environmental cooling. It is often desirable and practical to apply heat by direct current (Joule heating) because of its simplicity and rapid response.

Active control methods include open-loop and closed-loop strategies (as discussed in Song and Ma 2003, 2007; Song and Quinn 2004; Song 2001a; Song et al. 1999, 2000, 2001, 2003a, b, 2011), as well as Sect. 8). Closed-loop strategies require measurement of relevant parameters, which could include actuator temperature, structural or mechanical displacement, structural strain, etc. Non-contacting temperature measurement can be very valuable due to the low heat capacity of small SMA actuators. Fiber optic strain measurement is also desirable due to the low thermal sensitivity. Many other application-specific parameters may be useful for active control, such as fluid parameters (temperature, pressure) for a system involving convective heating and cooling or dynamic fluid loading.

A well-designed control system can have numerous advantages for the SMA system. It enables multiple output states such as position, mitigates some failure modes, and allows the designer to optimize the SMA performance and system design. Parts of the SMA control system include the SMA element (wire, tube, etc.), thermal elements (heating and cooling elements), sensors (output displacement sensor), and controller software and hardware. The control system design is intimately tied to the actuation form and actuation mode. The model of the SMA element is challenging because of the inherent nonlinearity and hysteretic relationship between input (temperature) and output (strain). Conventional control hardware and controller designs, such as Proportional-Integral-Derivative, computer based control, are often implemented for

SMA applications. However, thermal management is a feature of SMA control that is not significant for many other actuators. Efficient thermal management is critical to the application success and should be one of the driving design criteria for the control system. The controller design is based on the system objectives, e.g., to minimize settling time, avoid overshoot, minimize power requirement, among others.

8 Case studies

The ensuing case studies demonstrate different actuator design processes performed by CASMART member organizations. In each review, the incorporation of design aspects and key findings thought to influence future SMA actuator development are summarized.

8.1 Active jet engine chevron

Chevrons are a proven technology for jet exhaust noise reduction. However, a trade-off of noise reduction at take off and thrust loss at cruise dictates the need for active/deployable chevrons. Parametric effects of jet-engine chevron systems were also poorly understood at the time of this work. The objective of this work was to develop active chevron technology to enable immersible chevron systems for studies of immersion amount and circumferential distribution in a wind tunnel at model scale. Motivation for this work is demonstrated by the jet engine simulator (JES) shown with static (immovable) chevrons in Fig. 6.

8.1.1 Evaluation

Testing of active chevron systems at model scale in a wind tunnel presented some unique challenges. The model was approximately 1:9 scale of a commercial transport aircraft engine, resulting in chevron planform dimensions of approximately 4.8 × 3.3 cm and a trailing-edge thickness of 0.076 cm or less. The trailing-edge thickness was of paramount importance due to scaling issues in the aeroacoustic noise production mechanisms. Previous experience with laminated composites having embedded SMA actuators suggested that the thickness constraint could be met while providing adequate control authority (Turner 2001). In-plane actuation via SMA materials was the only approach known to have potential for achieving a deformable structure with the thickness constraint. Additionally, the temperature range and required cyclic frequency were within acceptable limits for known SMA materials and actuator forms.

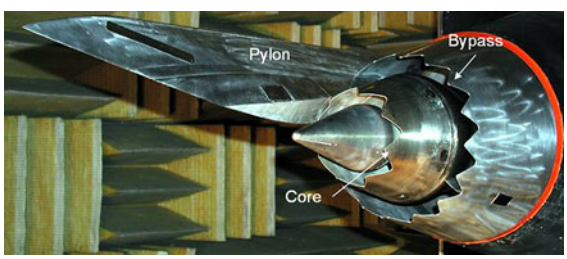

Fig. 6 JES with static, core and bypass chevrons

8.1.2 Alloy selection

The facility intended for testing the active chevron system was the NASA Langley Research Center (LaRC) Low Speed Aeroacoustic Wind Tunnel (LSAWT). The LSAWT is an open-circuit, open-jet acoustic wind tunnel equipped with a JES. The facility had provisions for forward flight simulation via the main tunnel flow and the JES had two engine flow streams representing core and bypass flows. The temperature of both engine flow streams was controllable, with a lower-limit on the bypass flow matching that of the freestream conditions. The active chevron treatment was restricted to the bypass nozzle to avoid the high temperatures associated with the core nozzle flow and thereby avoid the necessity for high-temperature SMA materials. These temperature considerations were the main discriminator in terms of alloy selection and the accommodations mentioned above allowed the use of typical, commercial SMA materials.

Other considerations such as the desire for high actuation authority and high electrical resistance, to facilitate the Joule heating, dictated a NiTi composition. Joule heating was selected to avoid the additional thickness of a surface-mounted heater and to localize the heating to the actuators. Furthermore, the thickness constraint and the desire to minimize the number of actuators, in order to achieve adequate actuation authority while simplifying fabrication and system integration, led to selection of a Nitinol material in a ribbon/rectangular-wire product form and having a thickness close to that of a typical composite ply. The selected material was a Nitinol alloy with a weight-percent composition of 55.4Ni-44.3Ti-0.3X, where X

indicates impurity content, in a ribbon product form with cross-sectional dimensions of 0.229 × 0.015 cm and having favorable transformation and shape memory characteristics, as will be described in more detail subsequently.

8.1.3 Actuator fabrication and processing

A laminated composite structure with embedded SMA actuators was envisioned to accomplish the objectives of this application. Consolidation of SMA actuators within the epoxy resin required a cure cycle at temperatures well above the expected actuator operating temperature in order to prevent the resin from softening too much during actuation. It was anticipated that such an elevated-temperature cure would compromise typical actuator "training" procedures, so the actuator performance was measured as a function of thermal cycle, see below, and the actuators were allowed to stabilize in the composite structure.

It was estimated from previous experimental data from the chosen Nitinol material that a prestrain of 4 % would result in sufficient actuation authority. Lengths of the prestrained SMA material were lightly sandblasted to remove the oxide layer for improved Nitinol–Nitinol joining and Nitinol-resin adhesion. The desire for Joule heating and the aerodynamic requirements, namely smooth integration of the chevron to the bypass nozzle and a geometrically-clean trailing edge, suggested the need for simple electrical connectivity to the actuators at the chevron root and provisions for one or more continuous electrical circuits within the chevron. Continuity within the chevron was provided by spot welds, made in an argon atmosphere, thereby joining pairs of Nitinol ribbon at strategic locations and forming an actuator subassembly that will be described in more detail in Sect. 7.

8.1.4 Testing and properties

Tests conducted on the Nitinol ribbon material included DSC to determine unconstrained transformation behavior, tensile tests at a range of temperatures and blocked-force tests as a function of temperature and thermal cycle. Tensile tests were conducted using an environmental chamber for temperature control. The cyclic, blocked-force testing was performed using Joule heating to increase the cyclic frequency. The data from these tests supported evaluation of the concept, first-order calculations for initial design, and "calibration" of numerical models for detailed design. The evolutionary behavior of the actuator material was quantified and used directly in lieu of training, as mentioned previously. Representative Young's modulus and recovery stress results are shown in Fig. 7. Additional detail on the test methods and results can be found in Turner (2001).

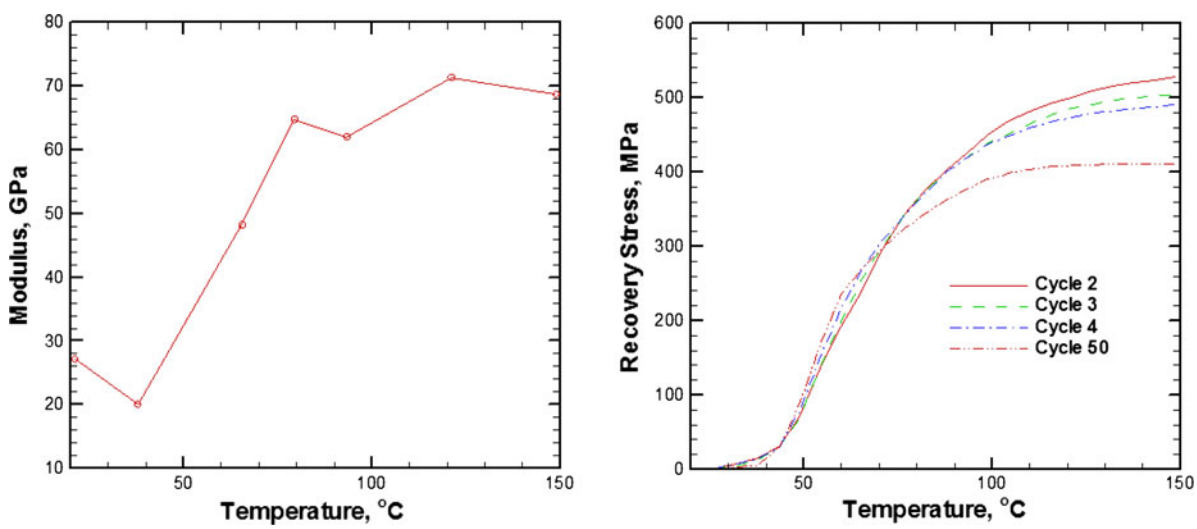

Fig. 7 Young's modulus and blocked-recovery-stress results from thermomechanical testing. (Color figure online)

8.1.5 Numerical modeling

A constitutive model that was particularly suited to modeling SMA actuators embedded in a laminated composite structure had recently been made available in commercial finite element codes (Turner 2000b; Turner and Patel 2005, 2007). Familiarity with the model and its relative simplicity made it possible to use the model for analysis and design throughout the active chevron project. Initial numerical studies were conducted on flat chevron concepts, i.e., without the cylindrical radius of curvature, to explore parameters such as number of composite layers, number of actuators and actuator placement. The desirable chevron bending movement was achieved simply by embedding the actuators on one side of the middle surface. Bending of a cylindrically curved chevron, however, required the actuators to be embedded so as to position the line of actuation toward the interior of the nozzle relative to the neutral axis, which does not lie on the middle surface. A schematic of a typical curved chevron, the neutral axis and the desirable embedded actuator configuration are shown in Fig. 8.

Computational results guided fabrication of chevron prototypes and were correlated with bench-top experimental results to make changes to the design or fabrication approach. Refinements in the computational model that were found to be important included accounting for laminate thickness variations, incorporating measured temperature distributions (from infrared thermography) and studying the influence of the aerodynamic load. A final design with predictable and acceptable performance was achieved using this approach.

8.1.6 System considerations

Integration of active chevrons into a wind-tunnel model required careful consideration of many factors including aerodynamics, electrical power distribution, instrumentation and control. The general fabrication process for the active chevrons consisted of lamination of oversized layers, consolidation by vacuum hot press and machining to final dimensions. Fabrication of an oversized laminate, as opposed to net-shape fabrication, allowed for the most flexibility in planform geometry and lay-up/cure tooling. Vacuum-hot-press processing facilitated rapid fabrication and high throughput. A glass–epoxy, unidirectional S2-glass/3501-6 resin) material system was selected because it was electrically insulating and allowed visual flaw detection. Material with a nominal cured ply thickness of 0.01 cm was selected to balance the objectives of low overall laminate thickness with high ply count to allow stiffness control and to facilitate actuator placement, i.e., maximize actuation authority.

A mold for the vacuum hot press was specifically designed to allow for a range of planform aspect ratios; see Fig. 9a. Glass–epoxy plies were cut to precise dimensions and lamination was performed to position the actuator assemblies as far from the neutral axis as possible. An actuator sub-assembly, processed as described above, is shown in Fig. 9b. A partial-ply was cut transversely and placed between the joined strips of SMA in each of the actuator sub-assemblies. This sub-assembly was aligned in the mold via a transparency template, as shown in Fig. 9c. The welds in each actuator sub-assembly were thus positioned near the intended tip of the chevron, while maintaining slight separation between the two actuator sub-assemblies at that location. Addition of the remaining plies finished out the lamination and lightly knurled

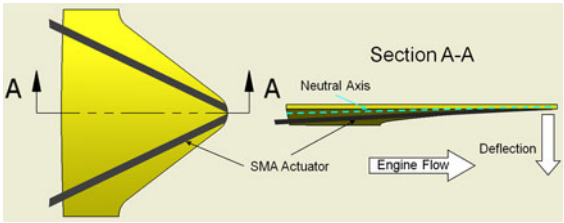

Fig. 8 Schematic of chevron and actuator configuration

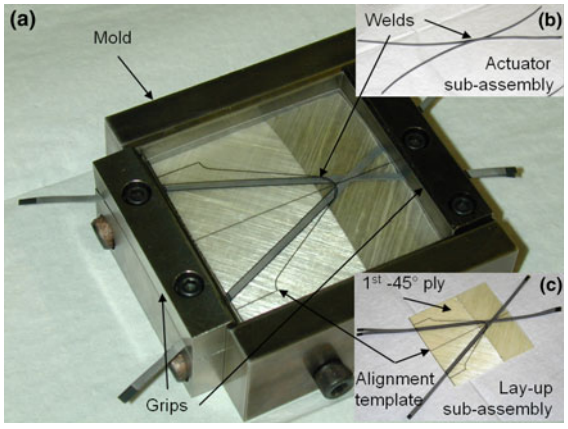

Fig. 9 Stages of the active chevron fabrication process: (*a*) laminate sub-assembly in mold; (*b*) actuator sub-assembly; (*c*) actuators positioned on laminate

grips in the fore and aft resin dams rigidly held the ends of the actuator sub-assemblies during the cure cycle. The thickness discontinuity at the actuator crossover point was accommodated by a hole cut in a layer of polyimide film that was placed in the mold beneath the laminate.

The portion of the actuator sub-assemblies protruding from the root of the consolidated laminate was copper plated to enable soldering and to improve contact-type electrical connections. The laminate was machined to the net-chevron shape by multiple passes of an end mill around the perimeter of a trim tool (to prevent delamination), as shown in Fig. 10a, thereby removing the sacrificial ends of the actuator sub-assemblies but leaving connectivity through the welds at the chevron tip. A chevron holder, shown in Fig. 10b, was designed to adapt the chevron to a typical bypass nozzle assembly for the LSAWT and to provide power and instrumentation connectivity to the chevron. The Cu-plated actuator ends were trimmed to fit the holder precisely with the bottom conductor of each actuator sub-assembly making contact with a Cu power lead. An electrical/mechanical clamp in the holder secured the actuator ends and provided connectivity between the two actuator sub-assemblies, thereby forming a single electrical circuit to power the entire chevron. Flame-sprayed aluminum oxide and polyimide film prevented unwanted connectivity within the holder and between the two conductors of each actuator sub-assembly at the chevron root, respectively. The active chevron is shown configured to test on the bench top and with representative flow via a square nozzle in Fig. 10c.

A PID-type controller was developed using structural strain, actuator temperature and flow properties (i.e., temperature and pressure), to control the immersion of the chevrons. The chevrons were individually fabricated and integrated into the nozzle with independent holders to allow for interchangeability and ease of replacement. Additional details on the active chevron development are available in (Turner et al. 2006, 2008).

8.2 High temperature SMA springs and wires

The design cycle for high-temperature (~300 °C actuation temperature) SMA springs and wires at NASA Glenn Research Center (GRC) was actuator-motivated rather than application-driven. That is, rather than designing to the specifications of a single application,

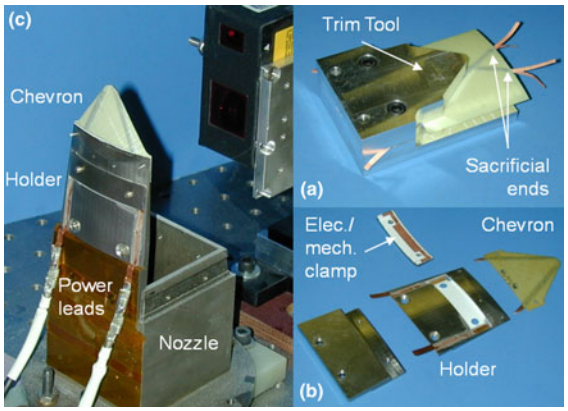

Fig. 10 Single chevron assembly: (*a*) machining to net shape; (*b*) mechanical/electrical connections; (*c*) bench-top/flow test apparatus

it was desired to arrive at a general class of actuators with quantified performance characteristics. This is somewhat different from the other case studies and design strategies documented within this article, but companies seeking to market actuators often adopt this alternate approach as a single development cycle yields actuators with many potential applications across multiple industries (e.g., Langbein 2009; Telezygology 2012; MigaMotors 2012). A great benefit is that subsequent application-specific design cycles are much less involved as the actuator is already established; akin to integrating a commercially available DC motor or pneumatic cylinder, controls and system integration are often the only further development required. Hence, this case study will follow the development of a suite of high-temperature SMA actuators through the stages that have been outlined in this article.

8.2.1 Evaluation

The decision to pursue a suite of high temperature SMA actuators was driven by NASA's successes in developing high temperature SMAs with promising properties and the potential for these new alloys to provide light-weight actuation in high-temperature environments where actuation is often challenging, such as near turbine cores.

8.2.2 Alloy selection

In years preceding this actuator development effort, metallurgists at GRC created a multitude of ternary

and quaternary NiTi-based high temperature SMA compositions and characterized their bulk actuation properties including transformation strain, thermal hysteresis, transformation temperatures, and cyclic accumulation of permanent set (i.e., "open loop strain") (Noebe et al. 2006, 2008; Bigelow 2006; Noebe et al. 2005; Bigelow et al. 2007, 2008a, b; Padula II et al. 2007; Padula et al. 2008). Of these alloys, $Ni_{19.5}Ti_{50.5}Pd_{25}Pt_5$ exhibited the most desirable combination of actuation properties, which included transformation temperatures ranging from 230 °C (M_f w/o load) to 350 °C (A_f under 400 MPa load) with a thermal hysteresis spanning ~80 °C, maximum transformation strain of ~2.8 %, and cyclic permanent set that did not exceed 0.5 % over 5,000 cycles provided the maximum temperature imposed upon the allo remained at or below 400 °C (Bigelow 2006; Padula II et al. 2007). Of all these properties, the cyclic stability was the primary influence on the decision to choose this alloy—other compositions had shown greater transformation strain in single cycles, but they had large permanent sets that did not stabilize with cycling, rendering them undesirable for use in applications (Bigelow 2006; Padula II et al. 2007). Here we note that high temperature SMA development efforts have continued at GRC since this suite of $Ni_{19.5}Ti_{50.5}Pd_{25}Pt_5$ actuators was developed, and a new $Ni_{50.3}Ti_{29.7}Hf_{20}$ alloy has shown a greater repeatable transformation strain of 3.5 % as well as superior cyclic stability (less than 10^{-3} % permanent set over hundreds of cycles) and a dramatically reduced thermal (20–25 °C) (Benafan 2012). The drawback to this alloy relative to $Ni_{19.5}Ti_{50.5}Pd_{25}Pt_5$ is that it may only be used in environments up to ~130 °C as it exhibits lower transformation temperatures.

8.2.3 Actuator fabrication and processing

Cylindrical 25.4 mm diameter by 102 mm long ingots were produced by VIM in a graphite crucible. The ingots were homogenized in vacuum at 1,050 °C for 72 h. and subsequently sealed inside an evacuated steel can in preparation for extrusion. 7:1 area reduction extrusion processes at 900 °C were then performed until the diameter of the SMA was reduced to 2.2 mm. To prevent Fe contamination, the steel cans were pickled off after each extrusion, and the material was then re-canned prior to the next extrusion. The 2.2 mm hot-extruded rods were centerless ground into wires of 1.5 and 1 mm diameters. To create 0.5 mm diameter wire, some of the 1.5 mm ground wires were annealed at 600 °C for 30 min and then cold-drawn to 0.5 mm diameter by Dynalloy, Inc.

Helical spring geometries (Table 2) were fabricated using these wires as starting material. Stainless steel mandrels were used as molds for the helical geometries, and the wires were wound around these mandrels, constrained to them using collets, and the clamped fixtures were then shape-set in a tube furnace using a heat treatment of 500 + 10 °C for 1 h. followed by air cooling. See Fig. 11 for a photo of mandrels, collets, and springs. To create the helical geometries of the smallest outside diameter (OD), it was necessary to first shape-set a spring of the larger OD, then wind and shape-set a spring around a smaller mandrel and shape set again. For the larger wire diameters, two intermediate diameter shape sets were required. Fracture occurred in attempts to create the smallest diameter springs directly from wire.

Table 2 Spring geometries that were fabricated and characterized in the development cycle of high temperature NiTiPdPt SMA actuators

Wire diameter (mm)	Spring OD (mm)
0.5	6.4
0.5	12.7
1.0	9.5
1.0	12.7
1.5	12.7
1.5	19.0

Fig. 11 Examples of the mandrels and collets discussed in the fabrication section of the high temperature SMA actuator case study, as well as some of the springs

8.2.4 Testing and properties

Details regarding the design and programming of the test fixtures used to characterize the actuators may be found in (Stebner 2007). Using this equipment, actuator components were subjected to a variety of dead loads and their displacement and temperature responses were recorded as electrical currents were turned on and off to thermally cycle the actuators through phase transformation. From these responses, transformation temperatures, strains, and stresses were documented using the methods described in Sect. 5.2 and the resulting data may be found in (Bigelow 2006; Padula II et al. 2007; Stebner 2007; Stebner et al. 2008, 2009). It was found that a maximum of actuation strain of $\sim$3 % was obtained from wires subjected to engineering tensile stresses of $\sim$400 MPa while the maximum stroke obtained from springs was observed when they were subjected to loads that result in shear stresses of 150–200 MPa in the undeformed helical geometries. Additionally, springs of smaller ODs are more efficient actuators than those of larger ODs as quantified by calculating work output per unit volume of material.

Also of interest was understanding the tradeoffs in choosing springs and wires of different geometries to facilitate reduced development times and costs for future engineering of high temperature SMA applications. To make these comparisons, wire and spring data were normalized to per unit length and per coil performances, respectively. This normalized data was then extrapolated to consider a 400 mm long wire of each diameter, as well as a spring made from that same 400 mm length of wire (Table 2). In examining this table, the benefits of each configuration are clear; wires can provide roughly double the total work output relative to springs, but that same wire turned into a spring can lead to over 1,500 % increase in stroke (Table 3).

8.2.5 Numerical modeling

The modeling used in the development cycle of these actuators was solely empirical. Geometrically it consisted of varying diameter for the wires and wire diameter, OD, pitch, and number of coils for the springs. Additionally, applied loads and currents were also varied to characterize responses under a variety of thermo-mechanical conditions.

Once the empirical database was developed, previously published SMA engineering models were evaluated to see if they could be used in selecting the best actuator for use in future applications. For wire form, a simple engineering model is sufficient to properly size actuators for application as the actuation stroke is now known for engineering stresses of 100, 200, 300, 400, and 500 MPa. Engineers may now design a $Ni_{19.5}Ti_{50.5}Pd_{25}Pt_5$ wire actuator by selecting a wire diameter that will carry the desired actuation load using the equation

$$F = \frac{\pi}{4}\sigma d^2 \tag{1}$$

knowing that the recommended operating stress to achieve maximum stroke using this material is between 350 and 400 MPa for lives of 10^2–10^3 cycles (It is possible lives will exceed this, but at this time cycles to failure for this developmental alloy are still largely unknown). The length of the wire may then be selected using the equation

$$l = \frac{stroke}{actuation\ strain}. \tag{2}$$

While engineering models do exist for design of SMA springs (e.g., Otsuka and Wayman 1998; Duerig et al. 1990), they were found to be insufficient to represent the characterized responses of the $Ni_{19.5}Ti_{50.5}Pd_{25}Pt_5$ springs, largely because these engineering models are formulated for small, linear-elastic-like deformations but the empirical study of

Table 3 Stroke and work capabilities of wires and springs (Stebner et al. 2009)

Wire diameter (mm)	Wire length (mm)	Wire max stroke (mm)	Wire work output (N × mm)	Spring OD (mm)	Spring max stroke (mm)	Spring work output (N × mm)
0.5	400	11	637	6.4	150	220
1	400	11	2,366	9.5	150	1,140
1.5	400	11	6,553	12.7	150	2,570

these springs showed highly non-linear, history dependent responses. Thus, if an application requires performance characteristics of a spring that do not fall within the established empirical database, a finite element simulation using a constitutive model formulated within a nonlinear thermodynamic framework is recommended.

8.2.6 System considerations

This stage of the design cycle was not specifically addressed in this effort as the goal was simply to characterize the performance of a suite of $Ni_{19.5}Ti_{50.5}Pd_{25}Pt_5$ SMA actuator components. However, integrating SMA wire and spring components is well documented (e.g., Duerig et al. 1990; Dynalloy 2011, Sect. 8.4). The only additional complication that arises with a high-temperature alloy is that of temperature: the electrical, mechanical, and thermal connections must be rated for temperatures up to 400 °C.

8.3 Oxygen mask deployment latch

To promote the future of SMA technology, SMA manufacturers such as Dynalloy, Inc. have often sponsored student design projects. Boeing has partnered with Dynalloy to support teams of Northwestern University undergraduate students in designing several SMA-actuated devices, including the lightweight latch-and-release mechanisms for deploying oxygen masks in the event of an emergency aboard commercial aircraft (see Fig. 12). The projects have been quite successful, as students have achieved over 75 % weight reduction from existing pneumatic cylinder and electric solenoid latches. Once implemented, this leads to an approximate weight savings of ~10 pounds per large aircraft (150+ seats), resulting in ~$150,000 fuel cost savings per vehicle each year the aircraft is in service (Maynard 2008).

While this case study reviews the development cycle in student projects, it also showcases the relative ease and simplicity that may be obtained in designing SMA actuation systems if commercially available products are able to fulfill the desired actuation requirements. Akin to the process of selecting a DC motor or pneumatic cylinder from a commercial vendor, properties and their relationship to geometries and configurations as well as system integration solutions are already developed and well documented, greatly reducing development times and costs.

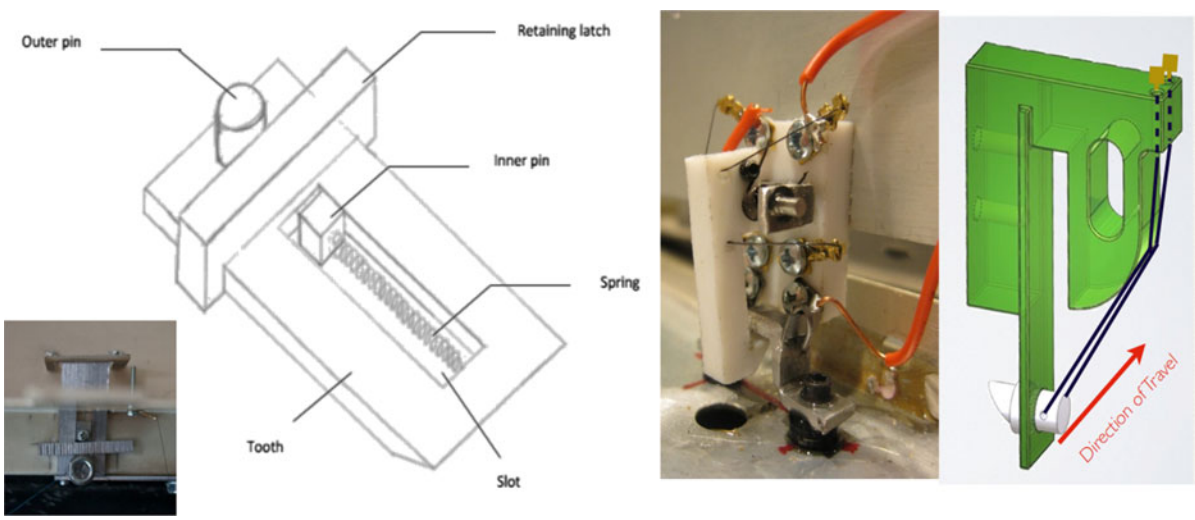

Fig. 12 Three student teams have independently designed SMA actuated latch-and-release mechanisms for stowing and deploying oxygen masks on commercial aircraft. Their designs reduce the weight of the pneumatic cylinders and electrical solenoids currently used by ~75 %. This leads to ~$150,000 in fuel savings per plane per year for large aircraft, such as the 747. The mechanisms are named (from *left to right*) *Compact Drop* (Spring 2011, Student Team: Matthew Chan, August Domel, Jerome Jeevarajan, Vineeth Raghunath), *Shape Memory Alloy Latch & Lever* (*SMALL*) (Spring 2010, Student Team: Gregory Budd, Michael Chen, Evan Hunt, Lyndon Sapozhnik), and *The Flex-i-Lever* (Spring 2010 Student Team: Frank Cummins, Jake Vander Ploeg, Ben Woldenberg)

8.3.1 Evaluation

In these projects, evaluation was performed for the students a priori. Boeing targeted these latches for weight reduction through application of advanced smart materials, one of which are SMAs. This target was set largely because a single, small (~0.1 mm diameter, 40–50 mm long) SMA wire has the potential to replace a (relatively) bulky, multi-component cylinder or solenoid and weight savings aboard any aircraft is paramount to reducing operating costs as well as CO_2 emissions.

8.3.2 Alloy selection

Dynalloy made their entire commercial offering of Flexinol® wires available to the students. This greatly accelerated the alloy selection process as the choice was reduced to "70" or "90 °C" wires. Most aircraft emergencies in which oxygen would be needed occur at high altitude as a result of cabin de-pressurization, thus the ambient temperatures are expected to be between −130 and 30 °C, depending on the nature of the emergency. In these cases, the 70 °C family of wires is most efficient since they require the least amount of thermal energy to actuate in these environments. However, one of the student teams considered the emergency of a cabin fire, and arrived at a different decision. In the event of fire, the ambient temperature could feasibly exceed 70 °C, and it would also be undesirable to feed the fire with extra oxygen. Thus the team decided to take advantage of a wire from each transformation temperature family: they used a 90 °C wire as the normal operation actuator, and justified the additional thermal energy need to operate it with the ability to use a 70 °C wire that would lock-out the oxygen masks if the compartments were near the fire (Fig. 13).

8.3.3 Actuator fabrication and processing

Dynalloy processed and fabricated crimped wire assemblies using their trade secrets.

8.3.4 Testing and properties

Dynalloy has published Technical Data Sheets (Dynalloy 2011) for their alloys, thus the base alloy properties were already determined for the students. The testing performed by the students mostly addressed configuration, control, and system integration issues. This testing was done in the Design and Mechatronics Laboratories at Segal Design Institute, Northwestern University, and was unique to each team's development goals. In general, the teams had to determine if their designed SMA configuration would work as anticipated, verify they had properly sized the biasing elements, and also determine the control parameters (current, time) required for repeatable actuation, which can vary from those published in Dynalloy's Tech Tips once the SMA component is thermally coupled to the system.

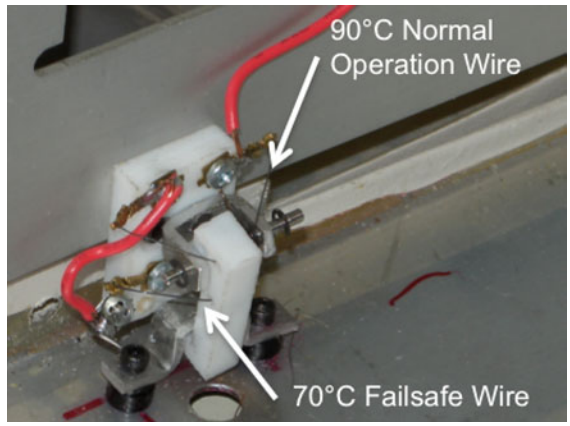

Fig. 13 A close-up view of the SMALL, which made use of both families of Flexinol® wires to provide a fail-safe that would prevent oxygen from being deployed into a burning fire

8.3.5 Numerical modeling

The students used first-order calculations aided by Dynalloy's Technical Data Sheets (Dynalloy 2011) to understand the performance strengths and tradeoffs of each configuration. For instance, they learned that if they fixed the ends of the wire and pulled on the wire's side they could achieve a larger stroke than if they used the wire in pure tension (14 vs. 5 % max), but the wire in the bending configuration could only accommodate a fraction of the operating force (~20 %). They also noted the electrical power requirements for using Joule heating to achieve actuation varied depending on wire length (higher resistance the longer the length) and diameter (higher resistance the smaller the diameter).

8.3.6 System considerations

The students took advantage of crimping solutions offered by Dynalloy to integrate the SMA wires both mechanically and electrically to the oxygen mask deployment systems. This highlights the advantages of using commercially available SMA solutions: they are well-developed and easy to implement relative to some of the other case studies documented in this article in which the SMA and/or actuator form was developed specifically for the application.

8.4 SMA-activated thermal switch for lunar surface applications

Thermal stability of Earth orbiting spacecrafts, space mission components (e.g., detectors, instruments, rovers, satellites, cryogen Dewars) and future outposts on the moon and Mars has been a critical constituent for reliable system operation. Several thermal solutions that are routinely employed on Earth are deemed impractical for space applications due to the high propulsive energy and cost required to transport payloads and store them in space. The objective of this work was focused towards developing a lightweight, self-sustained thermal switch that can benefit all space mission components where a heat path must be regulated during system operation. Particularly, the thermal switch designed, fabricated and tested in this work was aimed toward providing on-demand heat load rejection from a liquid oxygen (LOX) tank maintained at 92 K as the temperature of the space environment varies from 40 to 400 K on the lunar surface. This will help ensure efficient transport/storage/transfer of LOX when critical temperatures are reached.

8.4.1 Evaluation

Among a list of devices used to achieve component thermal stability, thermal switches have been at the forefront. Gas-gap, paraffin, and differential thermal expansion thermal switches have been developed and used (Martins et al. 2011), which provided the added benefit of coupling/decoupling capabilities and thermal isolation. Nevertheless, these devices usually depend on external resources (e.g., sensors, power, pumps and heaters) which increase system footprints and mass, in addition to mission cost. By replacing the switching mechanisms with solid-state "smart" actuators, considerable improvements in the overall system performance can be achieved. An SMA-activated thermal switch operates based on a fundamental material response that integrates sensing, control and actuation functions in a single entity. Since operation via SMAs is achieved through a material response and not mechanical or electrical actuation, a significant reduction in design complexities and input power requirements is possible. Moreover, SMA activated thermal switches operate in a spark-free and clean motion avoiding any faulting or ignition that can interrupt the continuity of operation. Examples of previously developed SMA switches based on conduction heat transfer principle are shown in Fig. 14.

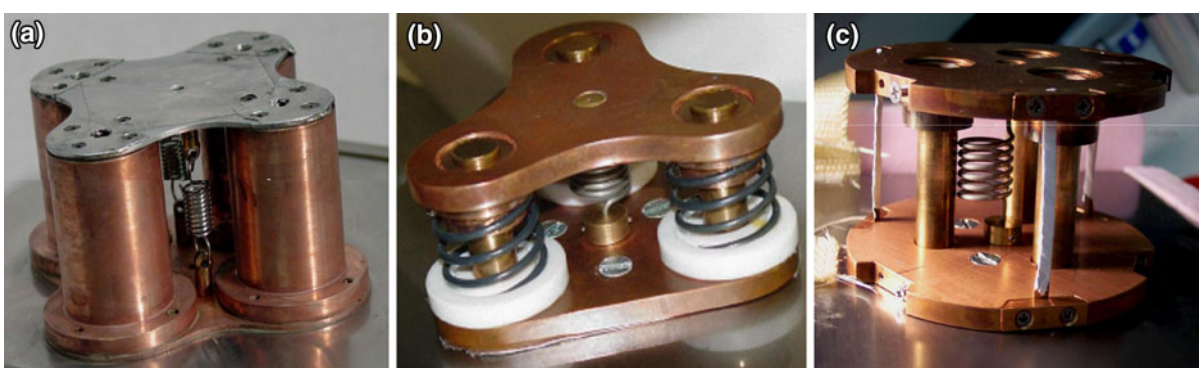

Fig. 14 SMA thermal conduction switch design progression as part of the University of Central Florida and NASA Kennedy Space Center collaboration. The actuation mechanisms of these switches are: **a** SMA housed helical-actuators (Droney et al. 2003), **b** SMA helical-actuators (Krishnan et al. 2008a), **c** SMA strip-actuators (Lemanski et al. 2006)

8.4.2 Alloy selection

From many classes of SMAs, near equiatomic NiTi is a commonly used SMA owing to its favorable mechanical properties (Funakubo 1987; Benafan 2012; Otsuka and Ren 2005; Ma et al. 2010) and commercial availability. Binary NiTi generally undergoes a cubic (B2) to monoclinic (B19′) phase transformation at temperatures from slightly below room temperature to around 100 °C (Otsuka and Wayman 1999), restricting the cold environment (below 0 °C) in which they can be used. Moreover, binary NiTi exhibits a wide thermal hysteresis associated with the phase transformation with significant dimensional instabilities during repeated thermomechanical cycling (Benafan 2012; Zarnetta et al. 2010). Addition of a third element such as iron (Fe) introduces a stable intermediate trigonal R-phase (B19′ ↔ R-phase ↔ B2) with improved fatigue response and reduced hysteresis while suppressing the phase transformation and shifting it to lower temperatures (Krishnan et al. 2008b; Otsuka and Ren 2005). As a tradeoff, strains associated with the R-phase are typically limited to about 1 % (compared to ~4–6 % in binary NiTi). Yet, SMAs can still be effectively developed as an actuator when used in the form of helical spring. These SMA spring elements can provide large strokes and adequate work output superior to conventional hydraulic or pneumatic actuators (Hirose et al. 1989; Mavroidis 2002; Frenzel et al. 2011). The selected material was a ternary $Ni_{47.1}Ti_{49.6}Fe_{3.3}$ (at.%) produced by Special Metals, New Hartford, New York (received in a spool of as-drawn 2.16 mm diameter wire). This alloy composition was selected based on a previous optimization study of different compositions and thermomechanical treatments, where it was found that these conditions provided the transformational properties of interest (Manjeri 2009).

8.4.3 Actuator fabrication and processing

The helical actuators were designed to function in extension (the "on" configuration) and compression (the "off" configuration) using torsion theory of close- and open-coiled helical springs under axial loading (Wahl 1963). Using NiTiFe wire (with a diameter, d, of 2.159 mm), the mean coil diameter, D, was selected to yield a spring index, C, of 7. Once the design was finalized through modeling (discussion follows), the as-drawn SMA wire was coiled around a solid mandrel with a helical groove. Shape setting was accomplished by heat treatment at 500 °C for 25 min., followed by an ice-water quench. The helical springs were then removed from the fixture and subjected to a final Electrical Discharge Machining (EDM) step to facilitate their fastening in the final assembly.

8.4.4 Testing and properties

The stress-free transformation temperatures: R-phase start (R_s), R-phase finish (R_f), austenite start (A_s), and austenite finish (A_f) were measured using a Perkin Elmer Diamond DSC at a rate of 20 °C/min under nitrogen cover gas. These temperatures were determined using the tangent intersection method and were found to be −10, −28, −25, and −6 ± 2 °C, respectively. The transformation from the R-phase to B19′ martensite was not detected in the temperature range tested, but it is expected to take place below −100 °C. Similar testing was performed after shape setting the actuators and after thermomechanical cycling. Thermomechanical characterization of the helical actuators was performed in a servo-hydraulic load frame for room temperature tests, and in a custom, fully instrumented vacuum bell jar for low temperature experiments. For the austenite phase, isothermal uniaxial tests at $A_f + 20$ °C were performed to determine the stress–strain response of the actuators. For the R-phase, the actuators were thermally cycled under constant loads between room temperature and −100 °C using controlled liquid nitrogen flow.

8.4.5 Numerical modeling

Adapting from Wahl (1963), the spring deflection, $\delta(T, \sigma)$, was determined according to:

$$\delta(T) = \frac{1}{4}\pi N_a D^3 F \sec\alpha \left[\frac{\cos^2\alpha}{G(T)J} + \frac{\sin^2\alpha}{E(T)I}\right] \quad (3)$$

where N_a is the number of active coils, α is the helix angle, $G(T)$ is shear modulus, $E(T)$ is the elastic modulus (dependent on the temperature T), J is the second polar moment of area and I is the second moment of area. As part of the design stage, a systematic methodology was developed with guidelines to devise efficient SMA helical actuators. Effects

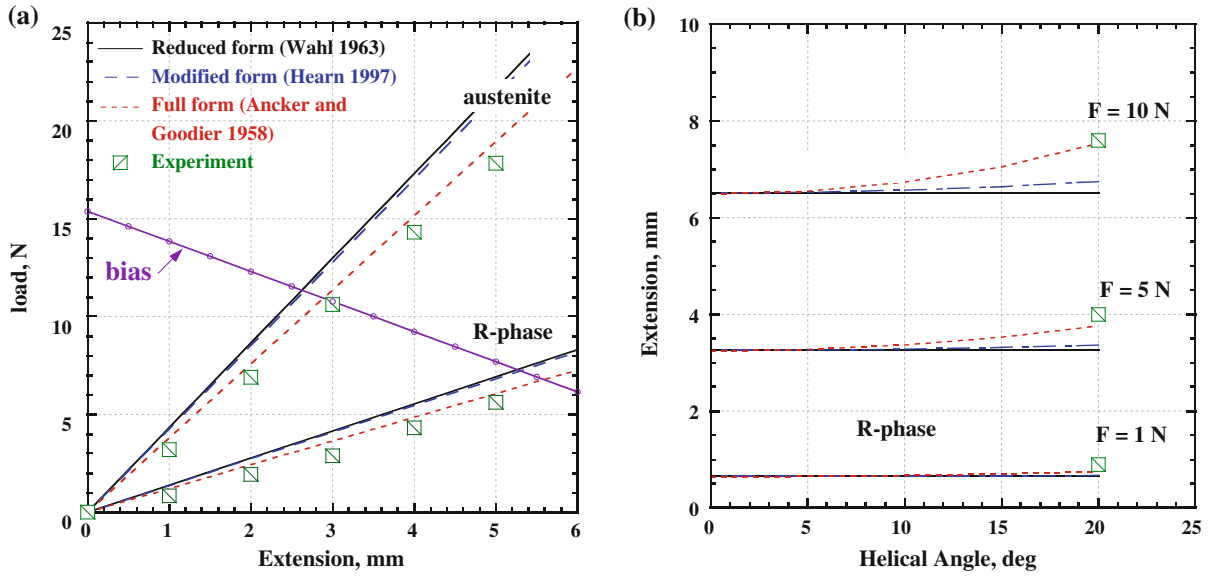

Fig. 15 Comparison of **a** load-extension and **b** extension-helix angle results obtained from theory and experiments. The reduced and modified formulations deviate from the experimental data at higher extensions and higher helical angles. (Color figure online)

of the helix angle were investigated by direct comparison between the reduced equations commonly employed (which neglects curvature and direct shear effects by assuming the spring elements as a straight wire in pure torsion) (Wahl 1963), modified models that account for the helix angle (Hearn 1997), and finally models in full form (Ancker and Goodier 1958) that account for bending and helix effects. A representative comparison between the three theoretical formulations and experiments is shown in Fig. 15. Detailed analyses with results can be found in Benafan (2008).

8.4.6 System considerations

The low temperature SMA actuators were combined with a variable length, two-phase heat pipe to construct the thermal switch. Two-phase heat pipes are advantageous in that they offer enhanced heat transfer and allow reductions in component weight and volume without decreasing performance. A schematic of the thermal switch operation is shown in Fig. 16. During a lunar day cycle ($\sim$ 14 days) when temperatures are near 400 K, the SMA actuators are in their open or "off" position and exist in their high temperature phase where they overcome the force from the bias springs (Fig. 16a). During a lunar night cycle when temperatures are near 40 K, the

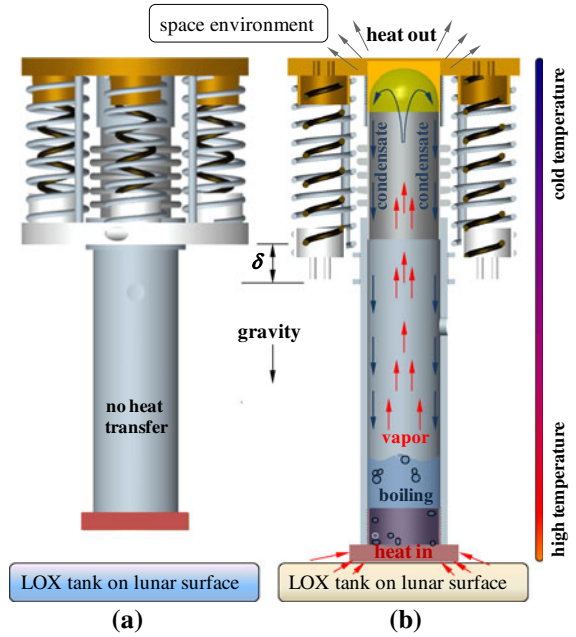

Fig. 16 Schematic of switch operation: **a** 'off' position during the lunar day (hot) and **b** 'on' position during the lunar night (cold)

temperature of the surrounding space environment drops resulting in a phase transformation in the SMA springs. The phase transformation results in the R-phase that is now less stiff and is overcome by the

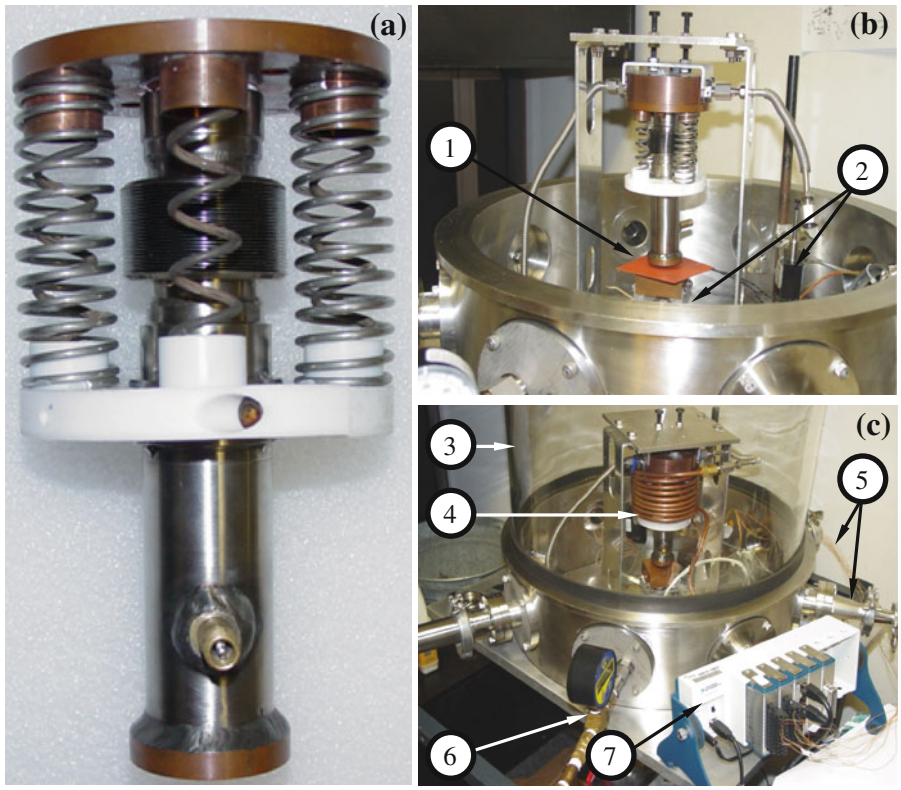

Fig. 17 **a** Variable length heat pipe switch with NiTiFe helical actuators and bellows. **b** Mounting fixture for testing. **c** Switch in instrumented vacuum bell jar (*1* heater; *2* LVDT for measuring stroke and load cell; *3* glass jar; *4* coils with liquid nitrogen; *5* thermocouples and power input through feed-throughs; *6* vacuum pump; *7* LabVIEW® data acquisition)

bias springs. The resulting actuation (facilitated by bellows in the heat pipe) takes the switch to its closed or "on" position wherein it is in thermal contact with the LOX tank as shown in Fig. 16b. In this closed position, heat is rejected by the heat pipe closed thermal process. As the temperature of the space environment increases, the SMA actuators retract and pull the switch back to the open or "off" position.

The complete assembly (Fig. 17a) was tested in an instrumented vacuum bell jar (Fig. 17b) where the actuation and thermal performance were acquired. Temperature was controlled to simulate working conditions by flowing liquid nitrogen and by heating elements inside the testing apparatus (Fig. 17c). Load, stroke, pressure, temperature and power were monitored and controlled using LabVIEW® for over 60 on–off cycles.

The thermal switch exhibited favorable and consistent thermo-mechanical properties while providing a reliable passive actuation mechanism. Large stroke during transformation (up to 7 mm) against bias forces (up to 39 N) with near-zero irreversible axial deformation were obtained. Integrating these actuators with a closed variable length two-phase heat pipe produced a thermal switch capable of transferring up to 13 watts using pentane as the working fluid. More detailed analyses and results can be found in Benafan (2008).

8.5 Variable geometry chevron

One source of noise from commercial high-bypass ratio turbofan engines is the turbulent mixing of the hot jet exhaust, fan stream, and ambient air. Serrated aerodynamic devices, or chevrons, immersed into the flow at the nacelle trailing edge have been shown to significantly lower jet noise at take-off and reduce shock cell noise during cruise (Calkins et al. 2006). The practical use of these devices requires a compromise between noise reduction and engine performance. While the immersed chevrons reduce noise,

their immersion also creates drag or thrust loss. These losses result in a penalty for flights with long cruise times. The VGC was developed to utilize compact, lightweight, and robust SMA actuators to morph the chevron between a shape optimized for noise reduction at takeoff and a shape at cruise that reduces shock cell noise without compromising engine performance (Calkins et al. 2006; Mabe et al. 2006b; Hartl et al. 2010c, d).

In August 2005, Boeing tested a number of noise reduction technologies on an All Nippon Airway (ANA) 777-300ER as part of the Quiet Technology Demonstrator-2 program (Fig. 18). The VGC thrust reverser translating sleeve was tested on a modified commercial GE90-115B engine. The VGC system was tested on six flights over 5 days with three different engine configurations. Autonomous operation and individual control of the 14 VGCs was demonstrated. Nine different chevron configurations were examined in the controlled mode, investigating both community noise and shock cell noise performance. The system was able to smoothly and quickly move between immersion configurations at cruise conditions, allowing a parametric study of chevron shapes for shock cell noise reduction. Test configurations included both uniform and azimuthally varying immersion configurations. In 2006 the VGC thrust reverser was modified for testing on a GE static engine test stand. Configurations similar to those conducted in flight were tested on a static engine stand (Calkins and Mabe 2007).

8.5.1 Evaluation

Morphing technologies increase a system's performance by manipulating characteristics to better match the system state to the operating conditions defined by the environment and task. The VGC allowed an optimized chevron shape at multiple flight conditions. In operation, the VGCs immerse into the engine fan flow to lower noise at takeoff and retract to reduce thrust losses at cruise. The SMA actuators were compact, lightweight, robust, thermally activated and thus uniquely suited to meet this morphing function.

The VGC design required a monolithic flexure actuator design to fit in the available space inside the chevron. While in the past a majority of the SMA based concepts and designs for morphing structures have used wire actuators, the simplicity of the monolithic flexure actuator is a great advantage. It has a very small part count and provides a simple, low-profile method of connecting to and deforming the substrate structure. It avoids the difficulties of wire based designs that often rely on a complex set of mechanisms and clamps to heat the wire and then transfer the large forces to the structure.

The VGC system was conceived of as having two modes of operation: powered and autonomous. In both modes, the SMA actuators are activated by thermal changes, driving a chevron shape change. During powered mode, a control system manages internal heaters to control the actuator temperature and corresponding VGC shape. The control system was used to continuously vary the chevron shape between the

Fig. 18 Flight test of VGC mounted on GE90-115B engine on a ANA 777-300ER as part of the Quiet Technology Demonstrator 2 program

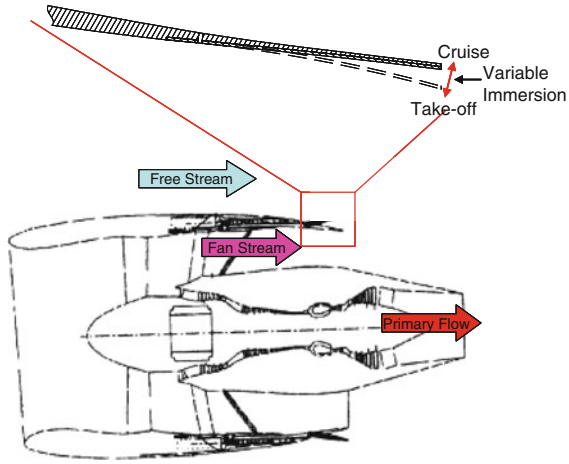

Fig. 19 Jet engine with VGC mounted on the trailing edge of the fan nozzle

actuation limits. This provided the ability to set and hold a chevron configuration of interest, facilitating a parametric study of the effect of chevron configurations on noise measurements. Strain gage signals provide a measure of each VGC's shape, quantified as a VGC tip immersion relative to the nozzle exit.

Autonomous mode relies on changes in environmental and fan exhaust temperatures to heat and cool the actuators. It requires no internal heaters, wiring, control system, or sensing. As illustrated in Fig. 19, this provided one tip immersion at take-off another during the cooler cruise state. According to specifications, the VGCs were required to produce a dynamic tip motion of over 0.9″, from 0.3″ into free stream to 0.6″ into fan stream.

8.5.2 *Alloy selection*

Until recently, highly Ni-rich NiTi alloys were not available commercially, however, research into the role of nickel in NiTi alloys has been under investigation for decades (Mabe et al. 2006a). Otsuka and Ren (2005) provide an outstanding overview of the field. They discuss in detail the background and current understanding of the development and effects of the secondary Ni-rich phases in NiTi alloys. Wojcik (2003) has completed work which examines the transition temperature, strain capability, and the effect of thermal aging on Ni-rich NiTi alloys. Boeing pioneered the use of the Ni-rich NiTi alloys for aerospace applications due to their unique properties. The Ni-rich NiTi alloys have excellent thermomechanical stability, their transition temperature can be set by a heat treatment process, and they do not require cold-work which allows for hot forming of complex shapes. A comparison of equiatomic and Ni-rich alloys shows that in tube form Nitinol-55 exhibits over twice the dynamic output of Nitinol-60 (Mabe et al. 2006a). However, the Ni-rich NiTi alloys have shown much greater dimensional stability under thermal mechanical cycling, thus making them useful as flexure actuator forms. Research with Nitinol-60 demonstrated that with proper heat treatment the same ingot of material could produce both superelastic and shape memory properties. Additionally with proper heat treatment, the transition temperatures could be varied from −55 to 70 °C. Recoverable strain up to 2.5 % has been observed along with a strong two way effect and high cyclic stability without cold work. More information on the history and properties of Nitinol-60 can be found in the references (Calkins and Mabe 2007; Mabe et al. 2006a; Otsuka and Ren 2005).

8.5.3 *Actuator fabrication and processing*

All of the flight test actuators were fabricated from a single billet of Nitinol-60 which had been hot rolled into nominally 0.25″ (0.635 cm) thick plate. The flexure's basic shape was formed in a series of water jet and wire EDM machining steps. The finished actuators were 10″ (25.4 cm) long by 1.5″ (3.8 cm) wide with smoothly varying thickness from 0.175″ (0.44 cm) at the middle to 0.06″ (0.15 cm) at both ends. Two holes were cut and tapped at the midpoint of each actuator for fastening to the substrate. The austenitic phase shape was set, the shape memory effect activated, and the transition temperatures established in a series of thermal processes. Figure 20

Fig. 20 Nitinol-60 flexure actuators used for flight test before (*bottom*) and after (*top*) heat treat processing

shows a pair of SMA flexure actuators before and after the final heat treatment processes.

Each actuator was conditioned for 100 thermal mechanical cycles while attached to a substrate nominally approximating the chevron substrate loads prior to installation on the chevron and system calibration. Thermally-induced plastic deformation is often a problem for applications employing SMAs. In the case of Nitinol-60, experience has shown that its austenitic set shape is significantly more stable than Nitinol-55. As with Nitinol-55, thermomechanical training can improve the stability of the transformation shapes, however with Nitinol-60 the number of training cycles required to stabilize the material is more than an order of magnitude less than conventional Nitinol-55. Figure 21 shows the test set up used for conditioning actuators which demonstrates the stable long term operation. The strain is plotted versus time for a prototype actuator thermally cycled on an aluminum substrate over the first 100 cycles.

8.5.4 Testing and properties

Initially the lack of data on monolithic Nitinol actuators, especially related to the effects of stress concentrations, varying stress and strain fields, and actuator-to-substrate interaction, made designing actuators difficult. This required a rigorous series of tests early in the program to produce material property data for design purposes and, most importantly, to meet flight requirements. The modulus of the NiTi alloy actuators was measured in two ways. The first method computed the Young's modulus by varying the applied stress and by measuring the strain while maintaining a constant temperature. The stress was applied at the tip of a cantilever beam for these characterization tests. The Young's modulus was calculated from the slope of the maximum beam stress versus maximum beam strain. The second method described in Fig. 22, involves thermally cycling the flexure under varying tip loads and plotting the fully austenite and the fully martensite applied stress versus strains for that particular cycle. The two methods return different values, particularly for the martensite state. The nature of these test methods, particularly the non-uniform stress and strain in a cantilever beam, and the inherent sample-to-sample variations in SMA properties makes it difficult to accurately derive bulk properties from this data; however it is an excellent predictor of the alloy's performance as an actuator (Mabe et al. 2006a).

8.5.5 Numerical modeling

The ability to adjust the transition temperature of Ni-rich NiTi with thermal processing makes it an ideal SMA for rapid prototyping projects where design and developmental time is limited or where the anticipated thermal environment is not well-known or defined. For conventional near equiatomic Nitinol the transition temperatures are set by the stoichiometry during billet production requiring that the actuators thermal specifications be set very early in a program. The ability to adjust the transition temperature of a single billet of Ni-rich NiTi significantly reduces the lead time required for finalizing thermal designs. This enabled the rapid development of the VGC for flight test by maintaining a great deal of flexibility in all aspects of the VGC thermal design. This unique property of

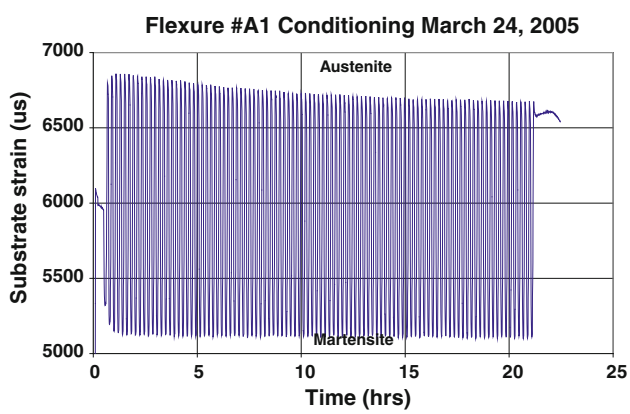

Fig. 21 SMA actuator conditioning set up and initial thermomechanical cycles

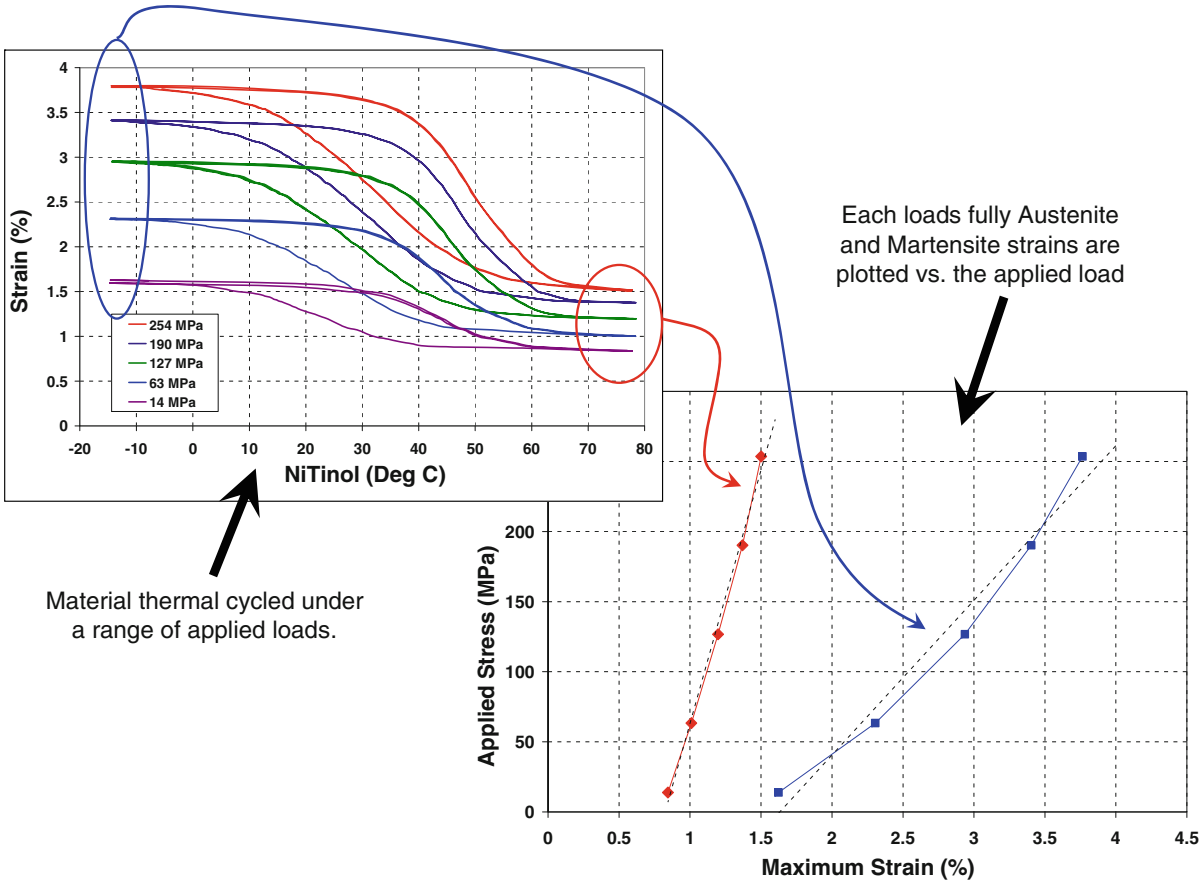

Fig. 22 Flexure test method. (Color figure online)

Nitinol-60 actuators made it possible to take the flight actuators and thermomechanically reprocess them and have an effective static engine test system. Reprocessing did not affect the actuator's fit inside the limited space of the chevron or the threaded holes used to connect the flexure actuators to the chevron substrate.

A Nitinol-60 cantilever beam tip displacement versus temperature hysteresis loop is shown in Fig. 23. For this Ni-rich NiTi alloy, the austenite start temperatures, defined as the temperature at which the material begins transitioning from martensite to the austenite phase, are seen to shift from less than 20 °C to more than 50 °C due to the variation in thermal processing methods (i.e., heat treatments). The same thermal processes applied to the Nitinol-55 produces only negligible changes in the transition temperatures. Similar trends have been reported in the literature (Wojcik 2003).

8.5.6 System considerations

The VGC program went from initial concept through several design and testing iterations before reaching a full scale flight test, Fig. 18. The full flight design included 14 chevrons integrated into the trailing edge of a GE90-115B thrust reverser's acoustic panel as shown in Fig. 18a. The GE90-115B thrust reverser consists of two primary structural elements, an inner and outer sleeve. The VGCs are an integral extension of the carbon composite inner sleeve. The basic design of the VGC was to embed low profile SMA actuators within a conventionally shaped chevron, with the same form factor as current fixed chevrons of interest. The SMA actuators are mated with the stiff chevron-shaped substrate forming the functional VGC as shown in Fig. 24. The chevrons had to be individually controlled and be able to change their immersion to produce a variety of configurations. On the finished

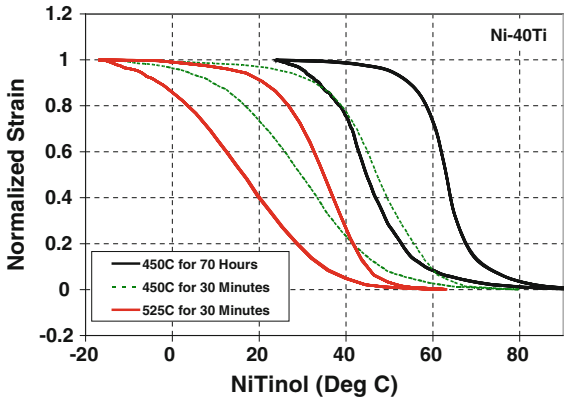

Fig. 23 Comparison of actuator strain-temperature hysteresis loops for varying heat treatments. (Color figure online)

thrust reverser sleeve, the sensor and power wiring passed through a conduit in the outer sleeve core, exited into a cavity between the inner and outer sleeve, and was then routed into the engine's fan case. The instrumentation wiring was terminated at a data system mounted in the fan case, while the power wiring continued down the wing and into the airplane cabin. A proportional-integral-derivative control system employed strain gages for position feedback and controlled the input to surface mounted heaters on the actuators.

8.6 Gas turbine variable area nozzle

The goal of using variable area nozzles for aero gas turbines has been considered since at least the 1950s, but practical considerations have limited them to applications where they are absolutely essential for engine operability as in super-sonic aircraft. More recently, they have been announced for the ultrahigh bypass Geared Turbofan engine (Mecham 2011) where it is also essential for operability. Gross performance benefits can be identified in established sub sonic engines, but the challenge is to recognize a net benefit when the implementation penalties such as weight and complexity are taken into consideration.

The basic properties of SMAs offer a very high energy density, simple actuation, full structural integration and smooth (flexural) shape change, but at the start of the project these properties were poorly controlled and understood, only available in small sections, and had not been demonstrated for larger scale high integrity engineering applications. The project challenge was to move every aspect towards practicality. Figure 25 shows a simple structure concept of a compound beam composed of an SMA outer skin attached to a thicker titanium skin. In this figure, the SMA outer skin is strained up to a maximum strain of 2 % in tension, which was devised to give a maximum material usage and ability for rapid cooling. Because the SMA outer skin is connected to the thicker titanium skin, this titanium skin experiences a bending strain of around 0.3 %, which is fully in the elastic range of this material, so therefore fully recoverable upon unloading. A typical element is shown in Fig. 25. Several elements can be optimized and concatenated to produce a component as in Fig. 26.

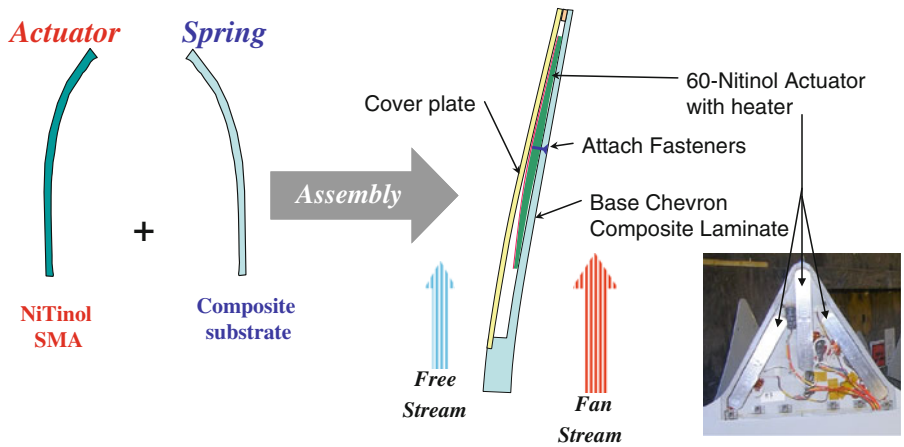

Fig. 24 Assembly of VGC showing key components

Major challenges were identified to move the concept towards a practical engineering application suitable for in-service use. Material size, consistency, temperature range and characterization were needed. Component design methods, machining, and joining to engineering standards and supply chain compatibility are essential.

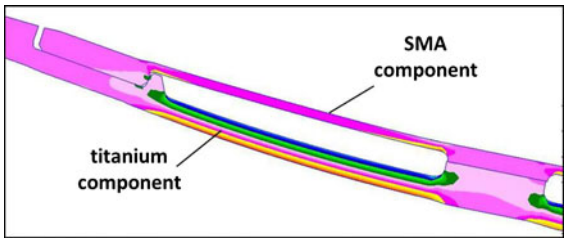

Fig. 25 Typical bender element and stressing model

Fig. 26 Sub element of SMA bender structure

8.6.1 Alloy selection

Wires with an equiatomic NiTi composition (e.g. Nitinol-55) were initially used due to ease of availability. Well-known composition sensitivity and casting segregation issues precluded expansion to larger sheets. Preliminary studies identified slightly Ti-rich variants as the way forward, although other studies (Frenzel et al. 2010) have subsequently indicated that Ni-rich would have been more appropriate. A Ti-rich NiTi alloy was developed to give a higher M_f and more homogeneous properties across large sheets. Sensitivity to exact composition has frequently been reported as causing severe difficulties in repeatability of properties, which was not expected with the Ti-rich NiTi alloy. New processing and characterization methods advanced this material, but it was only when fully representative testing was developed and carried out that drift in the stress plateau caused by accumulated strain and a significant reduction in M_f temperature indicated that a stable target life of 120 000 cycles could not be achieved. Therefore, an alloy consisting of $Ni_{41}Ti_{50}Cu_9$ (at.%) was selected due to its low thermal hysteresis, superior functional fatigue stability, and its potential availability on a commercial scale as a more attractive alternative to equiatomic NiTi. This revelation was only possible with the processing and testing techniques developed during the initial part of the program. Requiring a sheet which is stressed predominantly in tension greatly simplified the characterization and design processes. Isobaric or

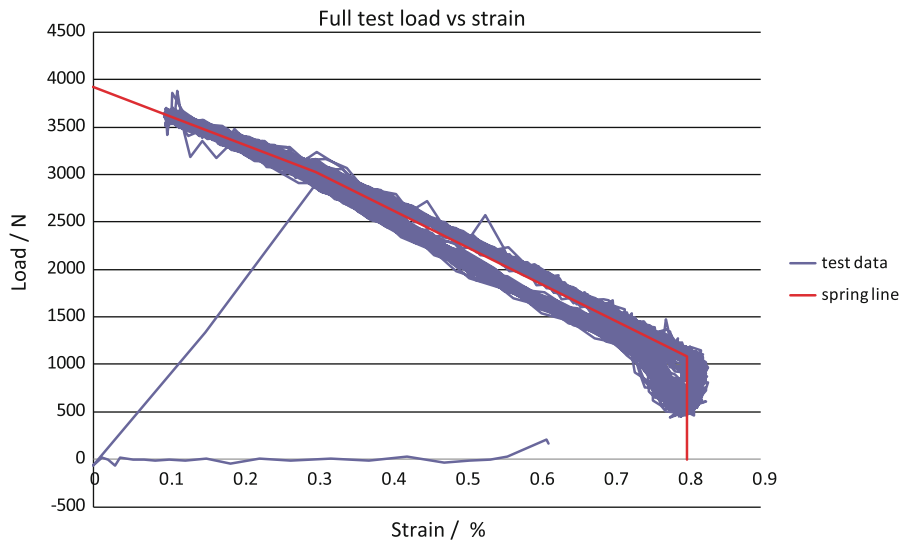

Fig. 27 Simulated spring line and end stop testing of NiTiCu sample. (Color figure online)

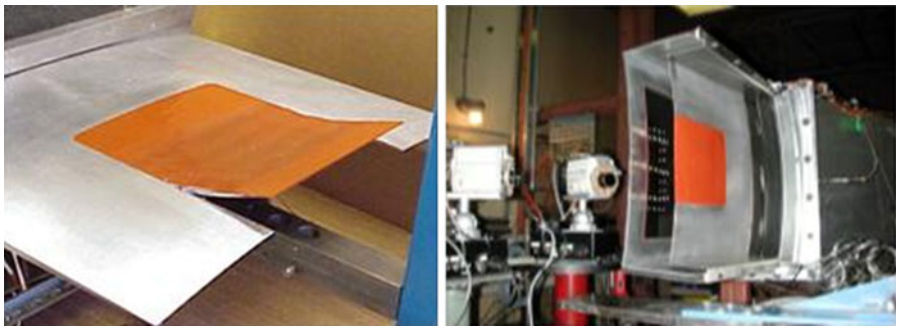

Fig. 28 Experimental component testing in wind tunnel (photo courtesy of Boeing)

isostatic testing is good for preliminary material selection, but a technique for controlled stress testing at two levels representing the hot and cold stresses resulted in major improvements. Progress to a fully representative spring line test with a high strain end stop (Fig. 27) achieved very stable operation. Thermomechanical pre-processing and cyclic stabilization of the material in sheets of approximately 450 × 250 × 3 mm was performed before machining in order to provide stable operation.

8.6.2 Actuator fabrication and processing, numerical modeling

The main challenges in component fabrication were around material stabilization and characterization as described above. Design methods worked through a bi-stable (hot or cold) beam model executed in a spread sheet with further optimization by FE methods (Fig. 25). Other issues followed good engineering practice for load reaction and the design of low stress joints. Current experimental components use mechanical fasteners, although brazing of the joint between NiTiCu and Ti6-4 alloy has been shown to be successful.

8.6.3 Testing and properties

Sub-element testing provided very useful data prior to production of a full scale nozzle segment which was subsequently tested in a wind tunnel at the Boeing Seattle plant (Fig. 28). The very stiff component performed well over full simulated flight cycles producing a tip displacement of 29.5 mm, this compares very well with the FE prediction of 30.1 and 31 mm from the spreadsheet model. The high stiffness is demonstrated by the achievement of less than 0.5 mm deflection under full aerodynamic loading.

8.6.4 System considerations

The use of SMA components in variable area nozzle design exhibit benefits from the identified gross performance improvement. The challenge, however, is to achieve a net benefit once all of the system issues have been considered whilst maintaining strict safety standards. These system issues include weight, aerodynamics, power, cost, and maintenance.

9 Conclusion

In this article, we have compiled the SMA actuation design experience to date of CASMART member organizations. From this collective experience, we developed a framework of six fundamental design aspects that may be used to structure the development of SMA actuation alloys and systems. We overviewed our experience with these aspects and demonstrated their application through six case studies. As with all technology, however, best practices and efficiency in development cycles are constantly being improved. Thus we have begun to incorporate this work into a living wiki (CASMART-DWG 2013) that may be used to access advancements to the state of the art.

In addition to these efforts toward facilitating SMA actuator design, CASMART has several other active efforts aimed at our larger mission of promoting SMA actuation technology. There is a modeling group that works to facilitate understanding and adoption of SMA models, such as those discussed in Sect. 6 (CASMART-MWG 2013). We also have a characterization group that is working toward solidifying standards for SMA actuation testing and properties. They outlined the foundation upon which these standards are being built in Sect. 5. The impact of

this work and future efforts is only as comprehensive and diverse as the contributing members of CASMART. Thus we welcome inquiry and involvement from others interested in these efforts.

Acknowledgments This work documents many years of effort from multiple organizations, encompassing support from numerous programs and funding agencies, and we thank them all. We also acknowledge CASMART's member institutions for their support of our consortium.

References

Achenbach, M., Muller, I.: Simulation of material behavior of alloys with shape memory. Arch. Mech. **37**(6), 573–585 (1985)

Ancker, C.J.J., Goodier, J.N.: Theory of pitch and curvature corrections for helical spring-I (tension). J. Appl. Mech. **25**, 471–479 (1958)

Antico, F.C., Zavattieri, P.D., Hector Jr, L.G., Mance, A., Rodgers, W.R., Okonski, D.A.: Adhesion of nickel-titanium shape memory alloy wires to thermoplastic materials: theory and experiments. Smart Mater. Struct. **21**(3), 035022 (2012)

Arghavani, J., Auricchio, F., Naghdabadi, R., Reali, A., Sohrabpour, S.: A 3-D phenomenological constitutive model for shape memory alloys under multiaxial loadings. Int. J. Plasticity **26**(7), 976–991 (2010)

ASTM-F2004-05: Standard Test Method for Transformation Temperature of Nickel-Titanium Alloys by Thermal Analysis, F2004-05 (2010)

ASTM-F2082-06: Standard Test Method for Determination of Transformation Temperature of Nickel-Titanium Shape Memory Alloys by Bend and Free Recovery. F2082-06 (2010)

Atli, K.C., Karaman, I., Noebe, R.D., Garg, A., Chumlyakov, Y.I., Kireeva, I.V.: Shape memory characteristics of $Ti_{49.5}Ni_{25}Pd_{25}Sc_{0.5}$ high-temperature shape memory alloy after severe plastic deformation. Acta Mater. **59**(12), 4747–4760 (2011)

Aydoğmuş, T., Bor, E.T., Bor, Ş.: Phase transformation behavior of porous TiNi alloys produced by powder metallurgy using magnesium as a space holder. Metall. Mater. Trans. A **42**(9), 2547–2555 (2011)

Bandeira, E., Savi, M., Monteiro, P., Netto, T.: Finite element analysis of shape memory alloy adaptive trusses with geometrical nonlinearities. Arch. Appl. Mech. **76**(3), 133–144 (2006)

Bansiddhi, A., Dunand, D.C.: Shape-memory NiTi foams produced by solid-state replication with NaF. Intermetallics **15**(12), 1612–1622 (2007)

Benafan, O., Noebe, R.D., Padula II, S.A., Gaydosh, D.J., Lerch, B.A., Garg, A., Bigelow, G.S., An, K., Vaidyanathan, R.: Temperature-dependent behavior of a polycrystalline NiTi shape memory alloy around the transformation regime. Scr. Mater. **68**(18), 571–574 (2013a)

Benafan, O., Padula II, S.A., Noebe, R.D., Brown, D.W., Clausen, B., Vaidyanathan, R.: An in situ neutron diffraction study of shape setting shape memory NiTi. Acta Mater. **61**, 3585–3599 (2013b)

Benafan, O., Vaidyanathan, R.: A shape memory alloy controlled heat pipe based thermal switch. In: Proceedings of ASME International Mechanical Engineering Congress and Exposition, Lake Buena Vista, vol. 11, pp. 107–109 (2009)

Benafan, O.: Deformation and phase transformation processes in polycrystalline NiTi and NiTiHf high temperature shape memory alloys. Ph.D. Dissertation, University of Central Florida (2012)

Benafan, O.: Design, fabrication and testing of a low temperature heat pipe thermal switch with shape memory helical actuators. M.S. Thesis, University of Central Florida (2008)

Benafan, O., Noebe, R.D., Padula II, S.A., Vaidyanathan, R.: microstructural response during isothermal and isobaric loading of a precipitation-strengthened Ni-29.7Ti-20Hf high-temperature shape memory alloy. Metall. Mater. Trans. A **43A**, 4539–4552 (2012a)

Benafan, O., Padula II, S.A., Noebe, R.D., Sisneros, T.A., Vaidyanathan, R.: Role of B19′ martensite deformation in stabilizing two-way shape memory behavior in NiTi. J. Appl. Phys. **112**(9), 093510 (2012b)

Bertacchini, O.W., Lagoudas, D.C., Patoor, E.: Fatigue life characterization of shape memory alloys undergoing thermomechanical cyclic loading. In: Proceedings of SPIE, Smart Structures and Materials: Active Materials: Behavior and Mechanics, San Diego, CA, pp. 612–624. doi:10.1117/12.508207 (2003)

Bertolino, G., Gruttadauria, A., Arneodo Larochette, P., Castrodeza, E.M., Baruj, A., Troiani, H.E.: Cyclic pseudoelastic behavior and energy dissipation in as-cast Cu-Zn-Al foams of different densities. Intermetallics **19**(4), 577–585 (2011)

Bhattacharya, K.: Microstructure of Martensite: Why It Forms and How It Gives Rise to the Shape-Memory Effect. Oxford Series on Materials Modelling. Oxford University Press, Oxford (2003)

Bhattacharya, K., Kohn, R.V.: Elastic energy minimization and the recoverable strains of polycrystalline shape-memory materials. Arch. Ration. Mech. Anal. **139**(2), 99 (1997)

Bigelow, G., Noebe, R., Padula, S., Garg, A., Olson, D.: Development and characterization of improved NiTiPd high-temperature shape-memory alloys by solid-solution strengthening and thermomechanical processing. In: SMST 2006: Proceedings of of the International Conference on Shape Memory and Superelastic Technologies, pp. 113–131 (2008a)

Bigelow, G.S., Gaydosh, D.J., Garg, A., Padula, S.A., Noebe, R.D.: Effects of stoichiometry on transformation temperatures and actuator-type performance of NiTiPd and NiTiPdX high-temperature shape memory alloys. In: SMST-2007: Proceedings of of the International Conference on Shape Memory and Superelastic Technologies, pp. 83–92 (2008b)

Bigelow, G.S., Padula, S.A., Garg, A., Noebe, R.D.: Correlation between mechanical behavior and actuator-type performance of Ni-Ti-Pd high-temperature shape memory alloys—art. no. 65262B. Proc. Soc. Photo-Optical Instrumentation, vol. 6526, B5262 (2007)

Bigelow, G.S.: Effects of Palladium Content, Quaternary Alloying, and Thermomechanical Processing on the Behavior of Ni-Ti-Pd Shape Memory Alloys for Actuator Applications. MS Thesis, Colorado School of Mines (2006)

Bigelow, G.S., Padula II, S.A., Garg, A., Gaydosh, D., Noebe, R.D.: Characterization of ternary NiTiPd high-temperature shape-memory alloys under load-biased thermal cycling. Metall. Mater. Trans. A **41**(12), 3065–3079 (2010)

Bigelow, G.S., Garg, A., Padula Ii, S.A., Gaydosh, D.J., Noebe, R.D.: Load-biased shape-memory and superelastic properties of a precipitation strengthened high-temperature Ni50.3Ti29.7Hf20 alloy. Scr. Mater. **64**(8), 725–728 (2011)

Bo, Z.H., Lagoudas, D.C.: Thermomechanical modeling of polycrystalline SMAs under cyclic loading, part III: evolution of plastic strains and two-way shape memory effect. Int. J. Eng. Sci. **37**(9), 1175–1203 (1999)

Boyd, J.G., Lagoudas, D.C.: A thermodynamical constitutive model for shape memory materials. 2. The SMA composite material. Int. J. Plasticity **12**(7), 843–873 (1996)

Brinson, L.C.: One-dimensional constitutive behavior of shape memory alloys: thermomechanical derivation with non-constant material functions and redefined martensite internal variable. J. Int. Mater. Syst. Struct. **4**, 229–242 (1993)

Brocca, M., Brinson, L.C., Bazant, Z.: Three-dimensional constitutive model for shape memory alloys based on microplane model. J. Mech. Phys. Solids **50**(5), 1051–1077 (2002)

Buehler, W.J., Wang, F.E.: A summary of recent research on the nitinol alloys and their potential application in ocean engineering. Ocean Eng. **1**(1), 105–120 (1968)

Burton, D.S., Gao, X., Brinson, L.C.: Finite element simulation of a self-healing shape memory alloy composite. Mech. Mater. **38**(5–6), 525–537 (2006)

Butera, F., Bianconi, E.: EP1031444—Control device with a shape memory actuating member heated by induction. Italy Patent (2000)

Calkins, F.T., Mabe, J.H.: Shape memory alloy based morphing chevrons: full scale static engine test. Paper No. AIAA-2007-3438. In: 13th AIAA/CEAS Aeroacoustics Conference, Rome, Italy (2007)

Calkins, F., Butler, G., Mabe, J.: Variable geometry chevrons for jet noise reduction, AIAA-2006-2546. In: 12th AIAA/CEAS Aeroacoustics Conference, Cambridge (2006)

Casati, R., Passaretti, F., Tuissi, A.: Effect of electrical heating conditions on functional fatigue of thin NiTi wire for shape memory actuators. Procedia Eng. **10**, 3423–3428 (2011)

Chan, C.W., Man, H.C.: Laser welding of thin foil nickel-titanium shape memory alloy. Opt. Laser. Eng. **49**(1), 121–126 (2011)

Chemisky, Y., Duval, A., Piotrowski, B., Ben-Zineb, T., Patoor, E.: numerical tool based on finite element method for SMA structures design. In: Smasis2008: Proceedings of the Asme Conference on Smart Materials, Adaptive Structures and Intelligent Systems—2008, vol. 1, pp. 411-419 (2009)

Chen, S., Craft, W.J., Song, D.Y.: Nonlinear adaptive control of dynamic systems driven by shape memory alloy (SMA) actuators. In: IMECE 2008: Mechanical Systems and Control, vol. 11, pp. 767–774 (2009)

CASMART-DWG: https://sites.google.com/site/casmartsmadesignwiki/home (2013)

CASMART-MWG. https://sites.google.com/site/smawiki/ (2013)

Coughlin, D.R., Phillips, P.J., Bigelow, G.S., Garg, A., Noebe, R.D., Mills, M.J.: Characterization of the microstructure and mechanical properties of a 50.3Ni-29.7Ti-20Hf shape memory alloy. Scr. Mater. **67**(1), 112–115 (2012)

Cross, W.B., Kariotis, A.H., Stimler, F.J.: Nitinol Characterization Study. In: NASA CR-1433 (1969)

Cui, D., Song, G.B., Li, H.N.: Modeling of the electrical resistance of shape memory alloy wires. Smart Mater. Struct. **19**(5), 055019 (2010)

Davis, B., Turner, T.L., Seelecke, S.: Measurement and prediction of the thermomechanical response of shape memory alloy hybrid composite beams. J. Int. Mater. Syst. Struct. **19**(2), 129–143 (2008)

DeCastro, J.A., Melcher, K.J., Noebe, R.D., Gaydosh, D.J.: Development of a numerical model for high-temperature shape memory alloys. Smart Mater. Struct. **16**(6), 2080–2090 (2007)

Dixon, J.R., Poli, C.: Engineering Design and Design for Manufacturing. Field Stone Publishers, Conway (1995)

Dolce, M., Cardone, D.: Mechanical behaviour of shape memory alloys for seismic applications. 2. Austenite NiTi wires subjected to tension. Int. J. Mech. Sci. **43**(11), 2657–2677 (2001)

Dow Corning Corporation: Silane Coupling Agents, Form No. 95-719-01 (2009)

Droney, M., Kaiboussi, N., Lemanski, J., Rodriguez, C., Woodruff, T.: Senior Design Project Report: Shape Memory Alloy Thermal Switch. University of Central Florida, Orlando (2003)

Duerig, T., Melton, K.: Wide Hysteresis NiTiNb Alloys. The Martensitic Transformation in Science and Technology. DGM Informationsgesellschaft, Oberursel (1989)

Duerig, T.W., Melton, K.N., Stoeckel, D., Wayman, C.M.: Engineering Aspects of Shape Memory Alloys. Butterworth-Heinemann, London (1990)

Dynalloy, Inc.: Technical Characteristics of Flexinol Actuator Wires, Dynalloy Inc., Tustin (2011)

Eggeler, G., Hornbogen, E., Yawny, A., Heckmann, A., Wagner, M.: Structural and functional fatigue of NiTi shape memory alloys. Mater. Sci. Eng. A **378**(1–2), 24–33 (2004)

Eggert, R.J.: Engineering Design. Pearson Prentice Hall, Upper Saddle River (2005)

Russell, S.M.: Nitinol melting and fabrication. In: Russell, S.M., Pelton, A.R. (eds.) SMST 2010: International Conference on Shape Memory and Superelastic Technologies, Pacific Grove, CA, USA, pp. 1–9 (2000)

Falvo, A., Furgiuele, F.M., Maletta, C.: Laser welding of a NiTi alloy: mechanical and shape memory behaviour. Mater. Sci. Eng. A **412**(1–2), 235–240 (2005)

Favier, D., Louche, H., Schlosser, P., Orgeas, L., Vacher, P., Debove, L.: Homogeneous and heterogeneous deformation mechanisms in an austenitic polycrystalline Ti-50.8 at.% Ni thin tube under tension. Investigation via temperature and strain fields measurements. Acta Mater. **55**(16), 5310–5322 (2007)

Figueiredo, A.M., Modenesi, P., Buono, V.: Low-cycle fatigue life of superelastic NiTi wires. Int. J. Fatigue **31**(4), 751–758 (2009)

Foroozmehr, A., Kermanpur, A., Ashrafizadeh, F., Kabiri, Y.: Effects of thermo-mechanical parameters on microstructure and mechanical properties of Ti-50 at.%Ni shape memory alloy produced by VAR method. Mater. Sci. Eng. A **535**, 164–169 (2012)

Frenzel, J., George, E.P., Dlouhy, A., Somsen, C., Wagner, M.F.X., Eggeler, G.: Influence of Ni on martensitic phase transformations in NiTi shape memory alloys. Acta Mater. **58**(9), 3444–3458 (2010)

Frenzel, J., Burow, J.A., Payton, E.J., Rezanka, S., Eggeler, G.: Improvement of NiTi shape memory actuator performance through ultra-fine grained and nanocrystalline microstructures. Adv. Eng. Mater. **13**(4), 256–268 (2011)

Fukumoto, S., Inoue, T., Mizuno, S., Okita, K., Tomita, T., Yamamoto, A.: Friction welding of TiNi alloy to stainless steel using Ni interlayer. Sci. Technol. Weld. Join. **15**(2), 124–130 (2010)

Funakubo, H.: Shape Memory Alloys. Gordon and Breach, New York (1987)

Furst, S.J., Seelecke, S.: Modeling and experimental characterization of the stress, strain, and resistance of shape memory alloy actuator wires with controlled power input. J. Int. Mater. Syst. Struct. **23**(11), 1233–1247 (2012)

Gall, K., Tyber, J., Wilkesanders, G., Robertson, S.W., Ritchie, R.O., Maier, H.J.: Effect of microstructure on the fatigue of hot-rolled and cold-drawn NiTi shape memory alloys. Mater. Sci. Eng. A **486**(1–2), 389–403 (2008)

Gao, X.J., Brinson, L.C.: SMA single crystal experiments and micromechanical modeling for complex thermomechanical loading. Smart Struct. Mater. **3992**, 516–523 (2000)

Gao, X., Brinson, L.C.: A simplified multivariant SMA model based on invariant plane nature of martensitic transformation. J. Int. Mater. Syst. Struct. **13**(12), 795–810 (2002)

Gao, X.: Multivariant Modeling and Characterization of SMAs Based on Hierarchical Characteristics of Martensite Crystallography. Northwestern University, Chicago (2002)

Gao, X.J., Huang, M.S., Brinson, L.C.: A multivariant micromechanical model for SMAs Part 1. Crystallographic issues for single crystal model. Int. J. Plasticity **16**(10–11), 1345–1369 (2000)

Gao, X., Brown, D.W., Brinson, L.C.: SMA texture and reorientation: simulations and neutron diffraction studies. In: Alison B. Flatau (ed.) Proceedings of SPIE. SPIE, San Diego, CA, pp. 715–726 (2005)

Gedouin, P.-A., Delaleau, E., Bourgeot, J.-M., Join, C., Arbab Chirani, S., Calloch, S.: Experimental comparison of classical PID and model-free control: position control of a shape memory alloy active spring. Control Eng. Pract. **19**(5), 433–441 (2011)

Gloanec, A.L., Cerracchio, P., Reynier, B., Van Herpen, A., Riberty, P.: Fatigue crack initiation and propagation of a TiNi shape memory alloy. Scr. Mater. **62**(10), 786–789 (2010)

Gollerthan, S., Young, M.L., Neuking, K., Ramamurty, U., Eggeler, G.: Direct physical evidence for the back-transformation of stress-induced martensite in the vicinity of cracks in pseudoelastic NiTi shape memory alloys. Acta Mater. **57**(19), 5892–5897 (2009)

Gravatt, L.M., Mabe, J.H., Calkins, F.T., Hartl, D.J.: Characterization of Varied Geometry Shape Memory Alloy Beams. Paper presented at the SPIE Smart Structures and Materials, San Francisco (2010)

Grossmann, C., Frenzel, J., Sampath, V., Depka, T., Oppenkowski, A., Somsen, C., Neuking, K., Theisen, W.: Processing and property assessment of NiTi and NiTiCu shape memory actuator springs. Materialwiss. Werkstofftech. **39**(8), 499–510 (2008)

Grummon, D.S., Shaw, J.A., Foltz, J.: Fabrication of cellular shape memory alloy materials by reactive eutectic brazing using niobium. Mater. Sci. Eng. A **438–440**, 1113–1118 (2006)

Gupta, K.: The Ni-Ti-Zr system (nickel-titanium-zirconium). J. Phase Equilib. **20**(4), 441–448 (1999)

Hartl, D.J. (2009): Modeling of Shape Memory Alloys Considering Rate-dependent Irrecoverable Strains. Texas A&M

Hartl, D., Zimmerman, T., Dilligan, M., Mabe, J., Calkins F.: Analysis of shape memory alloy components using beam, shell, and continuum finite elements. In: Proceedings of the ASME Conference on Smart Materials, Adaptive Structures and Intelligent Systems, vol. 1, pp. 295–305 (2010a)

Hartl, D.J., Stebner, A.P., Chemisky, Y., Benafan, O., Brinson, L.C.: A framework for the unified calibration of 3D phenomenological shape memory alloy constitutive models. Smart Mater. Struct. submitted (ASME-SMASIS Special Issue) (2012)

Hartl, D.J., Lagoudas, D.C.: Constitutive modeling and structural analysis considering simultaneous phase transformation and plastic yield in shape memory alloys. Smart Mater. Struct. **18**(10), 104017 (2009)

Hartl, D.J., Chatzigeorgiou, G., Lagoudas, D.C.: Three-dimensional modeling and numerical analysis of rate-dependent irrecoverable deformation in shape memory alloys. Int. J. Plasticity **26**(10), 1485–1507 (2010a)

Hartl, D.J., Lagoudas, D.C., Calkins, F.T., Mabe, J.H.: Use of a Ni60Ti shape memory alloy for active jet engine chevron application: I. Thermomechanical characterization. Smart Mater. Struct. **19**, 015020 (2010b)

Hartl, D.J., Mooney, J.T., Lagoudas, D.C., Calkins, F.T., Mabe, J.H.: Use of a Ni60Ti shape memory alloy for active jet engine chevron application: II. Experimentally validated numerical analysis. Smart Mater. Struct. **19**(1), 015021 (2010c)

Hartl, D.J., Lagoudas, D.C., Calkins, F.T.: Advanced methods for the analysis, design, and optimization of SMA-based aerostructures. Smart Mater. Struct. **20**(9), 094006 (2011)

Hassan, M.R., Scarpa, F., Mohamed, N.A., Ruzzene, M.: Tensile properties of shape memory alloy chiral honeycombs. Phys. Status Solidi (b) **245**(11), 2440–2444 (2008)

He, Y.J., Sun, Q.P.: Scaling relationship on macroscopic helical domains in NiTi tubes. Int. J. Solids Struct. **46**(24), 4242–4251 (2009)

Hearn, E.J.: Mechanics of Materials—An Introduction to the Mechanics of Elastic and Plastic Deformation of Solids and Structural Materials, 3rd ed., vol. 1. Elsevier, Amsterdam (1997)

Hirose, S., Ikuta, K., Umetani, Y.: Development of a shape memory alloy actuator. Improvement of output performance by the introduction of a s-mechanism. Adv. Robot. **3**, 3–16 (1989)

Hodgson, E.D.: Fabrication, Heat treatment and joining of nitinol components. In: Russell, S.M., Pelton, A. (eds.) Shape Memory and Superelastic Technologies (SMST), Pacific Grove, CA, pp. 11–24

Hsieh, S.F., Chen, S.L., Lin, H.C., Lin, M.H., Chiou, S.Y.: The machining characteristics and shape recovery ability of Ti-Ni-X (X = Zr, Cr) ternary shape memory alloys using the wire electro-discharge machining. Int. J. Mach. Tool. Manuf. **49**(6), 509–514 (2009)

Huang, M., Brinson, L.C.: Multivariant model for single crystal shape memory alloy behavior. J. Mech. Phys. Solids **46**(8), 1379–1409 (1998)

Huang, M.S., Gao, X.J., Brinson, L.C.: A multivariant micromechanical model for SMAs. Part 2. Polycrystal model. Int. J. Plasticity **16**(10–11), 1371–1390 (2000)

Iadicola, M.A., Shaw, J.A.: An experimental setup for measuring unstable thermo-mechanical behavior of shape memory alloy wire. J. Int. Mater. Syst. Struct. **13**(2–3), 157–166 (2002)

Ipek Nakas, G., Dericioglu, A.F., Bor, S.: Fatigue behavior of TiNi foams processed by the magnesium space holder technique. J. Mech. Behav. Biomed. **4**(8), 2017–2023 (2011)

Jackson, C.M., Wagner, H.J., Wasilewski, R.J.: 55-Nitinol the alloy with a memory: its physical metallurgy, properties, and applications. In: NASA SP-5110 (1972)

Kelly, A., Bhattacharya, K.: A constitutive model for shape-memory alloys that accounts for initiation, reorientation, and saturation. J. Mech. Phys. Solids (submitted, 2012)

Khamei, A.A., Dehghani, K.: A study on the mechanical behavior and microstructural evolution of $Ni_{60wt\%}Ti40_{wt\%}$ (60Nitinol) intermetallic compound during hot deformation. Mater. Chem. Phys. **123**(1), 269–277 (2010)

Kim, J.I., Miyazaki, S.: Effect of nano-scaled precipitates on shape memory behavior of Ti-50.9at.%Ni alloy. Acta Mater. **53**(17), 4545–4554 (2005)

Kohl, M., Dittmann, D., Quandt, E., Winzek, B., Miyazaki, S., Allen, D.M.: Shape memory microvalves based on thin films or rolled sheets. Mater. Sci. Eng. A **273–275**, 784–788 (1999)

Kong, M.C., Axinte, D., Voice, W.: Challenges in using waterjet machining of NiTi shape memory alloys: an analysis of controlled-depth milling. J. Mater. Process. Technol. **211**(6), 959–971 (2011)

Kovarik, L., Yang, F., Garg, A., Diercks, D., Kaufman, M., Noebe, R.D., Mills, M.J.: Structural analysis of a new precipitate phase in high-temperature TiNiPt shape memory alloys. Acta Mater. **58**(14), 4660–4673 (2010)

Krishnan, V.B., Bewerse, C., Notardonato, W.U., Vaidyanathan, R.: A thermal conduction switch based on low hysteresis NiTiFe shape memory alloy helical springs. AIP Conf. Proc. **986**(1), 3–9 (2008a)

Krishnan, V.B., Manjeri, R.M., Clausen, B., Brown, D.W., Vaidyanathan, R.: Analysis of neutron diffraction spectra acquired in situ during mechanical loading of shape memory NiTiFe at low temperatures. Mater. Sci. Eng. A **481–482**, 3–10 (2008b)

Lagoudas, D.: Shape memory alloys : modeling and engineering applications, 1st edn. Springer, New York (2008)

Lagoudas, D.C., Entchev, P.B., Popov, P., Patoor, E., Brinson, L.C., Gao, X.J.: Shape memory alloys, part II: modeling of polycrystals. Mech. Mater. **38**(5–6), 430–462 (2006)

Lagoudas, D.C., Miller, D.A., Rong, L., Kumar, P.K.: Thermomechanical fatigue of shape memory alloys. Smart Mater. Struct. **18**(8), 085021 (2009)

Langbein, S.: Development of standardised and integrated shape memory components in "one-module"—design. In: ESOMAT 2009—8th European Symposium on Martensitic Transformations (2009)

Lemanski, J.L., Krishnan, V.B., Manjeri, R.M., Notardonato, W.U., Vaidyanathan, R.: A low hysteresis NiTiFe shape memory alloy based thermal conduction switch. Adv. Cryog. Eng. **52**(1), 3–10 (2006)

Lexcellent, C., Bourbon, G.: Thermodynamical model of cyclic behaviour of Ti-Ni and Cu-Zn-Al shape memory alloys under isothermal undulated tensile tests. Mech. Mater. **24**(1), 59–73 (1996)

Li, M.G., Sun, D.Q., Qiu, X.M., Liu, J.B., Miao, K., Wu, W.C.: Effects of silver based filler metals on microstructure and properties of laser brazed joints between TiNi shape memory alloy and stainless steel. Sci. Technol. Weld. Join. **12**(2), 183–188 (2007)

Li, H., Yuan, B., Gao, Y., Chung, C.Y., Zhu, M.: High-porosity NiTi superelastic alloys fabricated by low-pressure sintering using titanium hydride as pore-forming agent. J. Mater. Sci. **44**(3), 875–881 (2009)

Li, H.M., Sun, D.Q., Cai, X.L., Dong, P., Wang, W.Q.: Laser welding of TiNi shape memory alloy and stainless steel using Ni interlayer. Mater. Des. **39**, 285–293 (2012)

Li, H., Sun, D., Cai, X., Dong, P., Gu, X.: Laser welding of TiNi shape memory alloy and stainless steel using Co filler metal. Opt. Laser Technol. **45**, 453–460 (2013)

Ma, N., Song, G.: Control of shape memory alloy actuator using pulse width (PW) modulation. In: Proc. Soc. Photo-Opt. Ins.: Smart Structures and Materials 2002: Modeling, Signal Processing, and Control, vol. 4693, pp. 348–359 (2002)

Ma, N., Song, G.: Control of shape memory alloy actuator using pulse width modulation. Smart Mater. Struct. **12**(5), 712–719 (2003)

Ma, N., Song, G., Lee, H.J.: Position control of shape memory alloy actuators with internal electrical resistance feedback using neural networks. Smart Mater. Struct. **13**(4), 777–783 (2004)

Ma, J., Karaman, I., Noebe, R.D.: High temperature shape memory alloys. Int. Mater. Rev. **55**, 257–315 (2010)

Mabe, J.H., Calkins, F.T., Butler, G.W.: Boeing's variable geometry chevron: morphing aerostructure for jet noise reduction, AIAA-2006-2142. In: 47th AIAA Adaptive Structures Conference Newport, RI (2006b)

Mabe, J., Ruggeri, R., Calkins, F.: Characterization of Nickel-Rich Nitinol Alloys for Actuator Development. In: SMST-2006: Proc. of the International Conference on Shape Memory and Superelastic Technologies, Pacific Grove, CA (2006a)

Malvern, L.E.: Introduction to the Mechanics of a Continuous Medium. Prentice-Hall Series in Engineering of the Physical Sciences. Prentice-Hall, Englewood Cliffs (1969)

Man, H.C., Zhao, N.Q.: Enhancing the adhesive bonding strength of NiTi shape memory alloys by laser gas nitriding and selective etching. Appl. Surf. Sci. **253**(3), 1595–1600 (2006)

Manjeri, R.M.: Low temperature and reduced length scale behavior of shape memory and superelastic NiTi and

NiTiFe alloys. Ph.D. Dissertation, University of Central Florida (2009)
Martins, D., Ribeiro, L., Lopes, D., Catarino, I., Esteves, I.A.A.C., Mota, J.P.B., Bonfait, G.: Sorption characterization and actuation of a gas-gap heat switch. Sens. Actuators A **171**(2), 324–331 (2011)
Mavroidis, C.: Development of advanced actuators using shape memory alloys and electrorheological fluids. Res. Nondestr. Eval. **14**(1), 1–32 (2002)
Maynard, M. (2008): To Save Fuel, Airlines Find No Speck Too Small. In: New York Times. NY, NY
Maziarz, W.: Structure changes of Co-Ni-Al ferromagnetic shape memory alloys after vacuum annealing and hot rolling. J. Alloy Compd. **448**(1–2), 223–226 (2008)
Mecham, M.: Smooth Start to GTF flight testing. In: Aviation Week and Space Technology, vol. 175, p. 40 (2011)
Mehrabi, K., Bruncko, M., Kneissl, A.C.: Microstructure, mechanical and functional properties of NiTi-based shape memory ribbons. J. Alloy. Compd. **526**, 45–52 (2012)
MigaMotors: http://www.migamotors.com (2012)
Mirzaeifar, R., DesRoches, R., Yavari, A.: A combined analytical, numerical, and experimental study of shape-memory-alloy helical springs. Int. J. Solids Struct. **48**(3–4), 611–624 (2011)
Mohammad, T., Jeng-Jong, R., Chuh, M.: Thermal post-buckling and aeroelastic behaviour of shape memory alloy reinforced plates. Smart Mater. Struct. **11**(2), 297 (2002)
Morin, C., Moumni, Z., Zaki, W.: Direct numerical determination of the asymptotic cyclic behavior of pseudoelastic shape memory structures. J. Eng. Mech. ASCE **137**(7), 497–503 (2011a)
Morin, C., Moumni, Z., Zaki, W.: Thermomechanical coupling in shape memory alloys under cyclic loadings: experimental analysis and constitutive modeling. Int. J. Plasticity **27**(12), 1959–1980 (2011b)
Neurohr, A.J., Dunand, D.C.: Mechanical anisotropy of shape-memory NiTi with two-dimensional networks of microchannels. Acta Mater. **59**(11), 4616–4630 (2011)
Nishida, M., Wayman, C., Honma, T.: Precipitation processes in near-equiatomic TiNi shape memory alloys. Metall. Mater. Trans. A **17**(9), 1505–1515 (1986)
Noebe, R., Draper, S., Gaydosh, D., Garg, A., Lerch, B., Penney, N., Bigelow, G., Padula, S., Brown, J.: Effect of thermomechanical processing on the microstructure, properties, and work behavior of a Ti(50.5)Ni(29.5)Pt(20) high-temperature shape memory alloy. In: SMST 2006: Proceedings of the International Conference on Shape Memory and Superelastic Technologies, 409-426 (2008)
Noebe, R., Gaydosh, D., Padula, S., Garg, A., Biles, T., Nathal, M.: Properties and potential of two (Ni,Pt)Ti alloys for use as high-temperature actuator materials. In: Proc. Soc. Photo-Opt. Ins.: Smart Structures and Materials 2005: Active Materials: Behavior and Mechanics, vol. 5761, pp. 364–375 (2005)
Noebe, R., Padula, S., Bigelowo, G., Rios, O., Garg, A., Lercf, B.: Properties of a Ni(19.5)Pd(30)Ti(50.5)high-temperature shape memory alloy in tension and compression—art. no. 617010. In: Proc. Soc. Photo-Opt. Ins.: Smart Structures and Materials 2006: Active Materials: Behavior and Mechanics, vol. 6170, p. 17010 (2006)
Novak, V., Sittner, P., Dayananda, G.N., Braz-Fernandes, F.M., Mahesh, K.K.: Electric resistance variation of NiTi shape memory alloy wires in thermomechanical tests: Experiments and simulation. Mater. Sci. Eng. A **481–482**, 127–133 (2008)
Oehler, S.D., Hartl, D.J., Turner, T.L., Lagoudas, D.C.: Modeling fluid structure interaction with shape memory alloy actuated morphing aerostructures. In: Proc. Soc. Photo-Opt. Ins.: Industrial and Commercial Applications of Smart Structures Technologies, vol. 8343 (2012b)
Oehler, S.D., Hartl, D.J., Lopez, R., Malak, R.J., Lagoudas, D.C.: Design optimization and uncertainty analysis of SMA morphing structures. Smart Mater. Struct. **21**(9), 094016 (2012)
Olsen, J.S., Zhang, Z.L., Lu, H., van der Eijk, C.: Fracture of notched round-bar NiTi-specimens. Eng. Fract. Mech. **84**, 1–14 (2012)
Olson, G.B., Cohen, M.: Mechanism for strain-induced nucleation of martensitic transformations. J. Less-Common Met. **28**(1), 107 (1972)
Olson, G.B., Owen, W.S.: Martensite : A Tribute to Morris Cohen. ASM International, Materials Park (1992)
Otsuka, K., Ren, X.: Recent developments in the research of shape memory alloys. Intermetallics **7**(5), 511–528 (1999)
Otsuka, K., Ren, X.: Physical metallurgy of Ti–Ni-based shape memory alloys. Prog. Mater Sci. **50**, 511–678 (2005)
Otsuka, K., Wayman, C.M.: Shape Memory Materials. Cambridge University Press, Cambridge (1998)
Otsuka, K., Wayman, C.M.: Shape Memory Materials. Cambridge University Press, Cambridge (1999)
Padula II, S.A., Noebe, R., Bigelow, G., Culley, D., Stevens, M., Penney, N., Gaydosh, D., Quackenbush, T., Carpenter, B.: Development of a HTSMA-actuated surge control rod for high-temperature turbomachinery applications. Paper presented at the AIAA adaptive structures conference, Waikiki (2007)
Padula, S., Bigelow, G., Noebe, R., Gaydosh, D., Garg, A.: Challenges and progress in the development of high-temperature shape memory alloys based on nitix compositions for high-force actuator applications. In: SMST 2006: Proceedings of the International Conference on Shape Memory and Superelastic Technologies, pp. 787–801 (2008)
Padula II, S., Qiu, S., Gaydosh, D., Noebe, R., Bigelow, G., Garg, A., Vaidyanathan, R.: Effect of upper-cycle temperature on the load-biased, strain-temperature response of NiTi. Metall. Mater. Trans. **43A**, 4610 (2012)
Panico, M., Brinson, L.C.: A three-dimensional phenomenological model for martensite reorientation in shape memory alloys. J. Mech. Phys. Solids **55**(11), 2491–2511 (2007)
Panico, M., Brinson, L.C.: Computational modeling of porous shape memory alloys. Int. J. Solids Struct. **45**(21), 5613–5626 (2008)
Patel, M.M., Gordon, R.F.: An investigation of diverse surface finishes on fatigue properties of superelastic nitinol wire. In: SMST 2006: Proceedings of the International Conference on Shape Memory and Superelastic Technologies, Pacific Grove, CA (2006)
Patoor, E., Bensalah, M.O., Eberhardt, A., Berveiller, M.: Micromechanical aspects of the shape memory behaviour. In: Proceedings of the International Conference on Martensitic Transformations (ICOMAT-92), pp. 401–406 (1993)

Patoor, E., Eberhardt, A., Berveiller, M.: Micromechanical modelling of the shape memory behavior. In: Brinson, L.C., Moran, B. (eds.) Mechanics of Phase Transformation and Shape Memory Alloys 1994, pp. 23–27. ASME, New York (1994)

Patoor, E., Lagoudas, D.C., Entchev, P.B., Brinson, L.C., Gao, X.J.: Shape memory alloys, part I: general properties and modeling of single crystals. Mech. Mater. **38**(5–6), 391–429 (2006)

Pourkhorshidi, S., Parvin, N., Kenevisi, M.S., Naeimi, M., Ebrahimnia Khaniki, H.: A study on the microstructure and properties of Cu-based shape memory alloy produced by hot extrusion of mechanically alloyed powders. Mater. Sci. Eng. A **556**, 658–663 (2012)

Qiu, S., Krishnan, V.B., Padula II, S.A., Noebe, R.D., Brown, D.W., Clausen, B., Vaidyanathan, R.: Measurement of the lattice plane strain and phase fraction evolution during heating and cooling in shape memory NiTi. Appl. Phys. Lett. **95**(14), 141906 (2009)

Qiu, S., Clausen, B., Padula II, S.A., Noebe, R.D., Vaidyanathan, R.: On elastic moduli and elastic anisotropy in polycrystalline martensitic NiTi. Acta Mater. **59**, 5055–5066 (2011)

Redmond, J.A., Brei, D., Luntz, J., Browne, A.L., Johnson, N.L.: Behavioral model and experimental validation for a spool-packaged shape memory alloy actuator. In: Proc. Soc. Photo-Opt. Ins.: Industrial and Commercial Applications of Smart Structures Technologies, San Diego, CA, pp. 693004–693013 (2008b)

Redmond, J.A., Brei, D., Luntz, J., Browne, A.L., Johnson, N.L.: Behavioral model and experimental validation for a spool-packaged shape memory alloy actuator—art. no. 693004. In: Proc. Soc. Photo-Opt. Ins.: Industrial and Commercial Applications of Smart Structures Technologies 2008, vol. 6930, p. 93004 (2008a)

Reedlunn, B., Shaw, J., Daly, S.: Vol. 1 of active materials, M.a.B.-h.M., simulation and control: shape memory alloy cables: exploratory experiments. In: Proceedings of the ASME 2009 Conference on Smart Materials, Adaptive Structures and Intelligent Systems (SMASIS 2009), Oxnard, CA, pp. 149–160 (2009)

Reedlunn, B., Shaw, J.: Shape memory alloy cables. In: Dapino, M.J., Ounaies, Z. (eds.) Proceedings of the SPIE 15th Annual International Symposium in Smart Structures and Materials, San Diego, CA, p. 69291G (2008)

Reedlunn, B., Shaw, J., Daly, S.: Pseudoelastic shape memory alloy cables. In: Grummon, D.S., Mitchell, M.R., Mertmann, M. (eds.) SMST 2010: Proceedings of the International Conference on Shape Memory and Superelastic Technologies, Pacific Grove, CA. New York: Springer (2010)

Resnina, N., Belayev, S., Voronkov, A.: Influence of chemical composition and pre-heating temperature on the structure and martensitic transformation in porous TiNi-based shape memory alloys, produced by self-propagating high-temperature synthesis. Intermetallics **32**, 81–89 (2013)

Sadjadpour, A., Bhattacharya, K.: A micromechanics-inspired constitutive model for shape-memory alloys. Smart Mater. Struct. **16**(5), 1751–1765 (2007)

Saleeb, A.F., Padula, S.A., Kumar, A.: A multi-axial, multi-mechanism based constitutive model for the comprehensive representation of the evolutionary response of SMAs under general thermomechanical loading conditions. Int. J. Plasticity **27**(5), 655–687 (2011)

Savi, M.A., Pacheco, P.M.C.L., Braga, A.M.B.: Chaos in a shape memory two-bar truss. Int. J. Nonlinear Mech. **37**(8), 1387–1395 (2002)

Schaffer, J.E., Plumley, D.L.: Fatigue performance of nitinol round wire with varying cold work reductions. J. Mater. Eng. Perform. **18**(5–6), 563 (2009)

Seelecke, S.: Modeling the dynamic behavior of shape memory alloys. Int. J. Nonlinear Mech. **37**(8), 1363–1374 (2002)

Sever, K., Sarikanat, M., Seki, Y., Tavman, I.H.: Concentration effect of γ-glycidoxypropyltrimethoxysilane on the mechanical properties of glass fiber–epoxy composites. Polym. Compos. **30**(9), 1251–1257 (2009)

Shaw, J.A.: Simulations of localized thermo-mechanical behavior in a NiTi shape memory alloy. Int. J. Plasticity **16**(5), 541–562 (2000)

Shaw, J.A., Kyriakides, S.: Initiation and propagation of localized deformation in elasto-plastic strips under uniaxial tension. Int. J. Plasticity **13**(10), 837–871 (1997a)

Shaw, J.A., Kyriakides, S.: On the nucleation and propagation of phase transformation fronts in a NiTi alloy. Acta Mater. **45**(2), 683–700 (1997b)

Shiue, R.H., Wu, S.K.: Infrared brazing of $Ti_{50}Ni_{50}$ shape memory alloy using two Ag-Cu-Ti active braze alloys. Intermetallics **14**(6), 630–638 (2006)

Smith, S.A., Hodgson, E.D.: Shape setting nitinol. In: Shrivastava, S. (ed.) Materials and Processes for Medical Devices Conference, Anaheim, CA, pp. 266–270 (2004)

Smith, N.A., Antoun, G.G., Ellis, A.B., Crone, W.C.: Improved adhesion between nickel-titanium shape memory alloy and a polymer matrix via silane coupling agents. Compos A Appl. Sci. **35**(11), 1307–1312 (2004)

Somsen, C., Zähres, H., Kästner, J., Wassermann, E.F., Kakeshita, T., Saburi, T.: Influence of thermal annealing on the martensitic transitions in Ni-Ti shape memory alloys. Mater. Sci. Eng. A **273–275**, 310–314 (1999)

Song, G.: Robust position regulation of a shape memory alloy wire actuator. Proc. Inst. Mech. Eng. I **216**(I3), 301–308 (2002)

Song, G., Chaudhry, V., Batur, C.: A new approach to the precision tracking control of shape-memory alloy actuators using neural networks and a sliding-mode based robust controller. In: Mater. Sci. Forum: Shape Memory Materials and Its Applications, vol. 394-3, pp. 83–86 (2001)

Song, G.: Robust position regulation of a rotary servo actuated by a shape memory alloy wire. In: ISIE 2001. IEEE International Symposium on Industrial Electronics Proceedings, pp. 1923–1928 (2001a)

Song, G.: Robust position regulation of a rotary servo actuated by a shape memory alloy wire. In: ISIE 2001: IEEE International Symposium on Industrial Electronics Proceedings, vols. I–III, pp. 1923–1928 (2001b)

Song, G.B., Kelly, B., Agrawal, B.N.: Active position control of a shape memory alloy wire actuated composite beam. In: Proc. Soc. Photo-Opt. Ins.: Smart Structures and Materials 1999: Mathematics and Control in Smart Structures, vol. 3667, pp. 755–766 (1999)

Song, G., Ma, N.: Control of shape memory alloy actuators using Pulse-Width Pulse-Frequency (PWPF) modulation. J. Int. Mater. Syst. Struct. **14**(1), 15–22 (2003)

Song, G.B., Ma, N.: Robust control of a shape memory alloy wire actuated flap. Smart Mater. Struct. **16**(6), N51–N57 (2007)

Song, G., Quinn, D.D.: Experimental study of the robust tracking control of a shape memory alloy wire actuator. J. Dyn. Syst. **126**(3), 674–677 (2004)

Song, G.B., Kelly, B., Agrawal, B.N.: Active position control of a shape memory alloy wire actuated composite beam. Smart Mater. Struct. **9**(5), 711–716 (2000)

Song, G., Chaudhry, V., Batur, C.: A neural network inverse model for a shape memory alloy wire actuator. J. Int. Mater. Syst. Struct. **14**(6), 371–377 (2003a)

Song, G., Chaudhry, V., Batur, C.: Precision tracking control of shape memory alloy actuators using neural networks and a sliding-mode based robust controller. Smart Mater. Struct. **12**(2), 223–231 (2003b)

Song, G.B., Ma, N., Li, L.Y., Penney, N., Barr, T., Lee, H.J., Arnold, S.: Design and control of a proof-of-concept active jet engine intake using shape memory alloy actuators. Smart Struct. Syst. **7**(1), 1–13 (2011)

Stebner, A.P.: Development, Characterization, and Application of NiTiPdPt High-Temperature Shape Memory Alloy Helical Actuators. The University of Akron, Akron (2007)

Stebner, A.P., Brinson, L.C.: Algorithms for explicit finite element implementation of a numerically improved three dimensional constitutive model for shape memory alloys. Comput. Methods Appl. Mech. Eng. **257**, 17–35 (2013)

Stebner, A., Padula, S.A., Noebe, R.D., Quinn, D.D. (2008): Characterization of $Ni_{19.5}Ti_{50.5}Pd_{25}Pt_5$ high-temperature shape memory alloy springs and their potential application in aeronautics—art. no. 69280X. In: Proc. Soc. Photo-Opt. Ins.: Active and Passive Smart Structures and Integrated Systems, vol. 6928

Stebner, A., Padula, S., Noebe, R., Lerch, B., Quinn, D.: Development, characterization, and design considerations of $Ni_{19.5}Ti_{50.5}Pd_{25}Pt_5$ high-temperature shape memory alloy helical actuators. J. Int. Mater. Syst. Struct. **20**(17), 2107–2126 (2009)

Stebner, A., Gao, X., Brown, D.W., Brinson, L.C.: Neutron diffraction studies and multivariant simulations of shape memory alloys: empirical texture development—mechanical response relations of martensitic nickel-titanium. Acta Mater. **59**(7), 2841–2849 (2011)

Stebner, A.P.: Ph.D. Dissertation, Northwestern University (2012)

Stebner, A.P., Brown, D.W., Brinson, L.C.: Young's modulus evolution and texture-based elastic-inelastic strain partitioning during large uniaxial deformations of monoclinic nickel-titanium. Acta Mater. **61**(6), 1944–1956 (2013)

Sun, Q.P., Hwang, K.C.: Micromechanics modeling for the constitutive behavior of polycrystalline shape memory alloys. 1. Derivation of general relations. J. Mech. Phys. Solids **41**(1), 1–17 (1993)

Sun, L., Zhao, Y., Huang, W.M., Tong, T.H.: Formation of combined surface features of protrusion array and wrinkles atop shape-memory polymer. Surf. Rev. Lett. **16**(06), 929–933 (2009)

Sun, L., Huang, W.M., Ding, Z., Zhao, Y., Wang, C.C., Purnawali, H., Tang, C.: Stimulus-responsive shape memory materials: a review. Mater. Des. **33**, 577–640 (2012)

Tanaka, K., Iwasaki, R.: A phenomenological theory of transformation superplasticity. Eng. Fract. Mech. **21**(4), 709–720 (1985)

Telezygology: http://www.tz.net (2012)

Thamburaja, P.: Constitutive equations for martensitic reorientation and detwinning in shape-memory alloys. J. Mech. Phys. Solids **53**(4), 825–856 (2005)

Thamburaja, P., Anand, L.: Polycrystalline shape-memory materials: effect of crystallographic texture. J. Mech. Phys. Solids **49**(4), 709–737 (2001)

Theisen, W., Schuermann, A.: Electro discharge machining of nickel-titanium shape memory alloys. Mater. Sci. Eng. A **378**(1–2), 200–204 (2004)

Tobushi, H., Hachisuka, T., Yamada, S., Lin, P.-H.: Rotating-bending fatigue of a TiNi shape-memory alloy wire. Mech. Mater. **26**(1), 35–42 (1997)

Turner, T.L.: Dynamic response tuning of composite beams by embedded shape memory alloy actuators. Smart Struct. Mater. **3991**, 377–388 (2000a)

Turner, T.L.: A new thermoelastic model for analysis of shape memory alloy hybrid composites. J. Int. Mater. Syst. Struct. **11**(5), 382–394 (2000b)

Turner, T.L. (2001): Thermomechanical Response of Shape Memory Alloy Hybrid Composites NASA/TM-2001-210656

Turner, T.L.: SMA hybrid composites for dynamic response abatement applications. J. Vib. Acoust. **127**(3), 273–279 (2005)

Turner, T.L., Patel, H.D.: Analysis of SMA hybrid composite structures in MSC.Nastran and Abaqus. J. Int. Mater. Syst. Struct. **18**, 435–447 (2007)

Turner, T.L., Patel, H.D.: Input Files and Procedures for Analysis of SMA Hybrid Composite Beams in MSC.Nastran and Abaqus. NASA/TM-2005-213517 (January 2005)

Turner, T.L., Buehrle, R.D., Cano, R.J., Fleming, G.A.: Modeling, fabrication, and testing of a SMA hybrid composite jet engine chevron concept. J. Int. Mater. Syst. Struct. **17**(6), 483–497 (2006)

Turner, T.L., Cabell, R.H., Cano, R.J., Silcox, R.J.: Development of a preliminary model-scale adaptive jet engine chevron. AIAA J. **46**(10), 2545–2557 (2008)

Wagner, M., Sawaguchi, T., Kaustrater, G., Hoffken, D., Eggeler, G.: Structural fatigue of pseudoelastic NiTi shape memory wires. Mater. Sci. Eng. A **378**(1–2), 105–109 (2004)

Wahl, A.M.: Mechanical Springs. McGraw-Hill, New York (1963)

Weinert, K., Petzoldt, V.: Machining of NiTi based shape memory alloys. Mater. Sci. Eng. A **378**(1–2), 180–184 (2004)

Weinert, K., Petzoldt, V., Kötter, D.: Turning and drilling of NiTi shape memory alloys. CIRP Ann. Manuf. Technol. **53**(1), 65–68 (2004)

Wessels, M., Hekman, E., Verkerke, B.: Influence of prestrain, heat treatment and surface treatment on bending fatigue of NiTi rod. J. Biomech. **45**(Suppl 1), 54 (2012)

Williams, E.A., Shaw, G., Elahinia, M.: Control of an automotive shape memory alloy mirror actuator. Mechatronics **20**(5), 527–534 (2010)

Wojcik, C.: Properties and heat treatment of high transition temperature Ni-Ti-Hf alloys. J. Mater. Eng. Perform. **18**(5), 511–516 (2009)

Wojcik, C.: Shape memory properties of nickel rich Ni-Ti alloys. In: Pelton, A., Hodgson, R., Duerig, T. (eds.) SMST 2003: International Conference on Shape Memory and Superelastic Technologies, pp. 43–52 (2003)

Wu, M.H.: Fabrication of nitinol materials and components. Mater. Sci. Forum **394–395**, 285–292 (2002)

Wu, K., Ma, J.L.: A review of high-temperature shape memory alloys. In: Russell, S.M., Pelton, A.R. (eds.) SMST 2000: International Conference on Shape Memory and Superelastic Technologies, Pacific Grove, CA, USA 2000, pp. 153–161 (2000)

Wu, S.K., Lin, H.C., Yen, Y.C., Chen, J.C.: Wire drawing conducted in the R-phase of TiNi shape memory alloys. Mater. Lett. **46**(2–3), 175–180 (2000)

Yamauchi, K., Ohkata, I., Tsuchiya, K., Miyazaki, S.: Shape Memory and Superelastic Alloys: Technologies and Applications. Woodhead Publications, Cambridge (2011)

Yan, X., Yang, D., Liu, X.: Electrochemical behavior of YAG laser-welded NiTi shape memory alloy. Trans. Nonferrous Met. Soc. **16**(3), 572–576 (2006)

Young, M., Wagner, M.-X., Frenzel, J., Schmahl, W., Eggeler, G.: Phase volume fractions and strain measurements in an ultrafine-grained NiTi shape-memory alloy during tensile loading. Acta Mater. **58**, 2344–2354 (2010)

Young, M.L., DeFouw, J.D., Frenzel, J., Dunand, D.C.: Cast-replicated NiTiCu foams with superelastic properties. Metall. Mater. Trans. A **43**(8), 2939–2944 (2012)

Zarnetta, R., Takahashi, R., Young, M.L., Savan, A., Furuya, Y., Thienhaus, S., Maaß, B., Rahim, M., Frenzel, J., Brunken, H., Chu, Y.S., Srivastava, V., James, R.D., Takeuchi, I., Eggeler, G., Ludwig, A.: Identification of quaternary shape memory alloys with near-zero thermal hysteresis and unprecedented functional stability. Adv. Funct. Mater. **20**(12), 1917–1923 (2010)

Zhang, Y., Jiang, S., Hu, L., Liang, Y.: Deformation mechanism of NiTi shape memory alloy subjected to severe plastic deformation at low temperature. Mater. Sci. Eng. A **559**, 607–614 (2013)

Zurbitu, J., Santamarta, R., Picornell, C., Gan, W.M., Brokmeier, H.G., Aurrekoetxea, J.: Impact fatigue behavior of superelastic NiTi shape memory alloy wires. Mater. Sci. Eng. A **528**(2), 764–769 (2010)